Resilient Cities and Structures 2 (2023) 1–17

Contents lists available at ScienceDirect

Resilient Cities and Structures

journal homepage: www.elsevier.com/locate/rcns

Full Length Article

# Structural connection with predetermined discrete variable friction forces

Kaixin Chen[1], Georgios Tsampras[1,*], Kyoungyeon Lee

*Department of Structural Engineering, University of California San Diego, 9500 Gilman Drive, La Jolla, CA 92093, USA*

ARTICLE INFO

*Keywords:*
Friction devices
Structural connections
Core wall buildings
Earthquake resilience

ABSTRACT

This paper presents a simple and practical structural connection able to develop predetermined discrete variable friction forces at target design displacement levels. The innovative connection is termed Modified Friction Device (*Modified FD*). Modified FDs are used to transfer the seismic induced horizontal forces from the floors to the core wall seismic force-resisting system of a building. The schematics of the physical embodiment of the Modified FD are presented. The components and the assembly of the Modified FD are discussed. The mechanics of the Modified FD are explained. Results from static structural analyses of two types of finite element models of the Modified FD are presented. The first model is developed using solid finite elements and it is used to assess the expected kinematics and the expected force-displacement response of the Modified FD. The second model is developed using a truss finite element and it can be used to efficiently simulate the force-displacement response of the Modified FD in numerical earthquake simulations of structural systems. The force-displacement response of the Modified FD computed using a numerical earthquake simulation of an eighteen-story reinforced concrete core wall building model is presented. The seismic response of the building model with Modified FDs is compared with the seismic response of the building model with monolithic connections and the seismic response of the building model with friction devices with constant friction forces. The results presented in this paper show that it is possible to develop a simple and practical structural connection with predetermined discrete variable force-displacement response to limit the seismic induced horizontal forces transferred between the floors of the flexible gravity load resisting system and the core wall piers in high-performance earthquake resilient buildings.

## 1. Introduction

### 1.1. Need for earthquake resilience

In February 2011, significant earthquake events occurred in Christchurch, New Zealand. One hundred and eighty-two fatalities and total damage of 18 billion US dollars were reported [1]. After the earthquake events, approximately 1240 buildings were demolished in the central city of Christchurch [2]. For five years, from 29 March 2011 until 18 April 2016, the Canterbury Earthquake Recovery Authority (CERA) led and coordinated the response and recovery efforts. This earthquake event is one out of the 905 large earthquakes reported from 1901 until 2015 [1]. The CRED/OFDA International Disaster Database from Université Catholique de Louvain, Brussels, Belgium [1] provides annual data related to the total deaths, the total damage, and the number of large earthquakes. Tsampras (2016) [3] analyzed the data and provided a plot of their cumulative normalized values as shown in Fig. 1. Fig. 1 also shows the normalized cumulative frequency of appearance of the word "*Resilience*" (defined in the following section) in the English corpus of Google Ngram between 1900 and 2008 [4]. The reported annual total number of large earthquakes was higher between 1980 and 2015 compared to previous years, possibly because of improved data collection. The word *Resilience* appeared more often in the literature during the same period of years compared to past years. The reported annual total damage was higher between 1980 and 2015 compared to past years, although it is possible that damage existed but was not included in the database [1]. Finally, between 1980 and 2015, the reported annual total deaths were significant compared to the past years. One might expect the reported annual total number of deaths and total damage to reduce over time considering the advancement of engineering knowledge and practice. However, the high concentration of population in earthquake-prone regions (e.g., the population in California doubled from 1960 to 2000 and continues to increase [5]) and the growth of infrastructure may explain the observed trend. Considering the above observations, it can be concluded that the data imply an increasing need for earthquake resilience.

### 1.2. US National earthquake resilience

US National earthquake resilience is one of the priorities of the National Earthquake Hazards Reduction Program (NEHRP) [6,7]. Accord-

* Corresponding author.
*E-mail address:* gtsampras@ucsd.edu (G. Tsampras).
[1] Authors with equal contribution.

https://doi.org/10.1016/j.rcns.2023.02.006
Received 15 December 2022; Received in revised form 10 February 2023; Accepted 12 February 2023
2772-7416/© 2023 The Author(s). Published by Elsevier B.V. on behalf of College of Civil Engineering, Tongji University. This is an open access article under the CC BY-NC-ND license (http://creativecommons.org/licenses/by-nc-nd/4.0/)

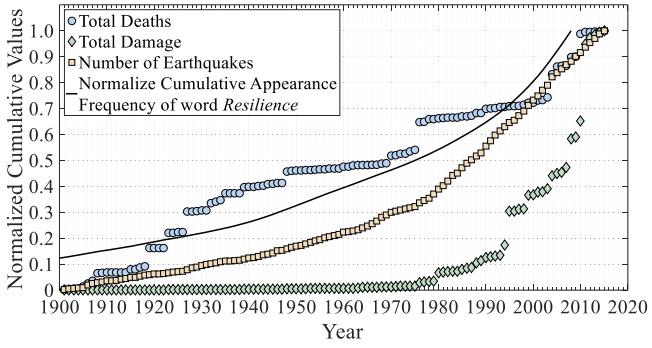



**Fig. 1.** Normalized cumulative annual total deaths, total damage, number of large earthquakes, and appearance frequency of the word *Resilience*.

ing to the National Research Council of the National Academies [8], "*A disaster-resilient nation is one in which its communities, through mitigation and pre-disaster preparation, develop the adaptive capacity to maintain important community functions and recover quickly when major disasters occur*". McAllister et al. [9] defined community resilience as "*the ability to prepare for anticipated hazards, adapt to changing conditions, and withstand and recover from disruptions*". The same authors stated that "*Even if a community enforces and adopts all current codes and standards, the performance of the built environment is not expected to result in a resilient community. This is because prescriptive and performance requirements in current codes and standards primarily focus on life safety objectives for buildings and transportation, and on reliability for electric and water*".

Designing individual buildings to recover at a functional level promptly after a strong earthquake event is required to contribute to community resilience and, as a result, enhance the national earthquake resilience. Individual buildings can be designed to return to a target functionality state after a given period if resilience-based design methods are used [7]. High-performance building systems can be utilized to mitigate the expected damage in the structural and non-structural components. In 2015, the Building Seismic Safety Council recommended research to advance the state of the art in earthquake-resistant building design [10] and identified issues in the current procedures used for the analysis and design of buildings. FEMA published issues and research needs related to the future development of the NEHRP Provisions and seismic design methods [11]. Key issues are associated with the "*Specific performance objectives and associated design criteria for performance beyond current code*" and provisions associated with "*better-than-code*" structural systems. Examples of "*better-than-code*" structural systems include buildings with components in their seismic load path that inherently can be designed to achieve high seismic performance compared to conventional building systems.

### *1.3. Uncertainty in seismic response of buildings and potential earthquake damage*

The design of conventional earthquake-resistant building systems is associated with uncertainty in the prediction of their seismic response. This uncertainty is a result of the variability in the earthquake ground motions, and the variability in the structural characteristics and their evolution in time, which in turn affects the nonlinear response of the building components [12–14]. More specifically, the variability in the seismic response of structural connections can be high due to the complex interactions resulting from the need to preserve kinematic compatibility between structural components. For example, the framing interaction between the floor diaphragms and the seismic force-resisting systems may lead to damage of the connection [15] that results in uncontrolled transfer of forces. Because of this uncontrolled response, the seismic induced horizontal forces in the floor diaphragms can be large relative to the floor diaphragm strength and may lead to a non-ductile response of the diaphragms [16]. The development of excessive seismic induced inertial forces can also produce inelastic responses and significant damage to the seismic force-resisting system [17,18]. More specifically, the loss of the ability of the connections of diaphragms to transfer forces to the seismic force-resisting system could lead to local collapse of the floor or complete collapse of the building [19–21]. After the 2010–2011 Christchurch earthquakes, excessive damage and collapse of floor diaphragms were attributed to inadequate integrity of the load path, underestimation of seismic-induced horizontal forces, and poorly understood interactions between floor diaphragms and walls, supporting beams, and reinforced concrete moment frames [22–24]. The damage repairs required after the 2010–2011 Christchurch earthquakes highlighted the need for the development of low-damage high-performance earthquake-resilient seismic force-resisting systems [25,26].

### *1.4. High-performance buildings and the effect of higher modes in the total dynamic response of buildings*

Kelly et al. [27,28], inspired by the bridge piers of the 200 ft high South Tangitikei railway bridge, provided a sketch of a "stepping wall" which acts as the seismic force-resisting system of the structure. This stepping wall has energy absorbers to control the response of the structure. Damage is concentrated on the energy absorbers that could be replaced after a strong ground motion. Since then, research has been conducted to develop seismic force-resisting systems with low post-earthquake damage and replaceable structural components. More specifically, researchers have developed post-tensioned moment-resisting frames [29–34], rocking structural wall systems [35–45], and rocking frame systems [46–51]. Summaries of high-performance earthquake-resilient seismic force-resisting systems developed to mitigate the damage of structural and nonstructural components are provided in the following references [52–55]. Alavi and Krawinkler showed that strengthening moment-resisting frames with walls that are able to pivot at their base instead of rocking mechanism can reduce the drift demands in a building [56]. Mar [57], Wada et al. [58], Qu et al. [59], and Janhunen et al. [60] presented examples of buildings that use vertical seismic force-resisting systems with rocking or pivoting base mechanism that prevents the localization of the story drift demand at a particular story in a frame building. "Strongbacks" or "spines" with a pivoting base mechanism have also been used in addition to energy dissipation mechanisms to resist the seismic induced horizontal forces, prevent the localization of the story drift demand at a particular story in a frame building [61–65], and limit the floor accelerations [66,67]. Fig. 2 shows sketches of example planar wall buildings with (a) flexural inelastic base mechanism, (b) rocking base mechanism, and (c) pivoting base mechanism. The sketch of the system with the pivoting base mechanism is based on the system proposed by Wada et al. [58].

The nonlinear response of the vertical elements of the seismic force-resisting system can act as a "cut–off" mechanism that may limit the floor accelerations and, as a result, limit the seismic induced horizontal inertial forces [68,69]. Even when the ductile nonlinear response of the seismic force-resisting system occurs, high floor accelerations may be observed, due to the uncontrolled forces transferred between the floors and the vertical elements of the seismic force-resisting system and the amplified response of second and higher modes [70]. Studies of buildings with seismic force-resisting systems that develop a flexural inelastic base mechanism (e.g., flexural-dominated reinforced concrete structural walls), a rocking base mechanism (e.g., rocking structural walls or controlled rocking braced frames), or a pivoting base mechanism show that high floor accelerations due to the contribution of the second-mode and higher-mode response in the total dynamic response (termed higher-mode effects) can be expected [46,52,71–74].

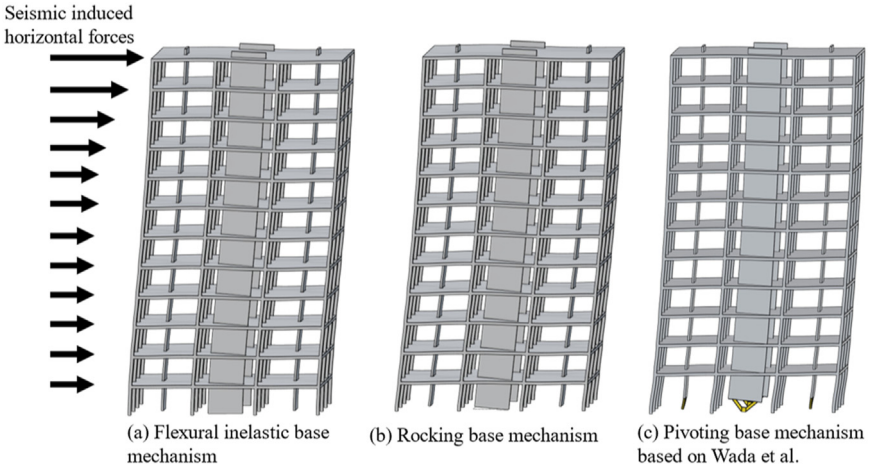



**Fig. 2.** Example planar wall buildings with (a) flexural inelastic base mechanism, (b) rocking base mechanism, and (c) pivoting base mechanism. The sketch of the system with the pivoting base mechanism is based on the system proposed by Wada et al..

### *1.5. Methods to limit the higher-mode effects*

Christopoulos and Zhong provided a review of the current state-of-the-art and state of research pertaining to the understanding, estimation, and mitigation of higher-mode effects on the seismic response of tall and slender RC structures [52]. To limit the higher-mode effects in high-rise structural wall buildings with flexural inelastic base mechanism, Panagiotou et al. [75] developed the dual-plastic hinge design concept which introduces a second plastic hinge along the height of the structural wall. To control the higher-mode effects in rocking frames, Wiebe et al. [73,74] proposed the use of multiple rocking mechanisms above the rocking base mechanism.

Practical force-limiting connections have been developed with goal to limit the seismic induced horizontal forces transferred from the floors to the vertical elements of planar seismic force-resisting systems in earthquake-resistant buildings and limit the higher-mode effects [3,76–84]. A force-limiting connection consists of a friction device or a buckling-restrained brace and low-damping rubber bearings. The force-limiting connections are designed to accommodate the seismic induced three-dimensional kinematic requirements between floors and planar seismic force-resisting systems. The low-damping rubber bearings provide out-of-plane stability to the planar walls of the seismic force-resisting system and post-elastic stiffness to the force-limiting connections. The post-elastic stiffness in the force-limiting connections limits the seismic induced displacement of the floors relative to the planar seismic force-resisting system. Fig. 3 shows a force-limiting connection that consists of a friction device and low-damping rubber bearings installed in an example building with rocking walls [79,80]. The seismic response of buildings with force-limiting connections between gravity load resisting systems and reinforced concrete planar walls [3,76–79,81], planar rocking walls [79,80,82–84], and self-centering concentrically braced steel frames [3,84] has been studied. The use of force-limiting connections in these buildings (1) limits the seismic induced force and acceleration responses, (2) reduces the variability in the force and acceleration responses due to the ground motion variability, and (3) mitigates the effects of higher-mode responses on the dynamic response of buildings [77]. Similar observations have been made for the seismic response of buildings with dissipative floor connectors between the gravity load resisting system and steel concentrically braced frames [85]. The dissipative floor connectors consist of rubber bearings and a friction device [86].

### *1.6. Friction-based force-limiting connections in core wall buildings*

Friction devices can be designed to be axially stiff, compact, and easy to manufacture and assemble. The design of friction devices is not limited by strain requirements similar to the strain requirements used in the design of metallic yielding devices. However, the friction force generated by a friction device depends on the materials used in the frictional interface, the sliding velocity, the cumulative sliding, the dwell time, and the manufacturing tolerances of the components of the friction device [79]. If properly designed, friction devices can remain undamaged during earthquakes, and they can be reused. Friction devices have been used in various structural applications. Clark et al. (1973) presented test results for a static load control friction device intended to limit the effect of differential settlement that occurs at foundations [89]. Researchers also used friction devices for energy dissipation in various types of earthquake-resistant structures, such as bridge structures [90], precast concrete structures [37,91–94,94–104], wall pier coupling beams [105,106], steel braced frames [107–116], steel moment resisting frames [117–123], self-centering moment resisting frames [33,124–128], and rocking timber shear walls [129–131]. Friction dampers [132–138], negative stiffness friction dampers [139,140], and self-centering braces with friction-based energy dissipation [141–145] have been developed and tested, as well.

The reinforced concrete core wall system is a widely used seismic force-resisting system for tall buildings because of its high lateral stiffness and its capacity for dissipating energy [146–151]. In addition to reinforced concrete, core walls can also be formed using cross-laminated timber structural walls [152] or concrete filled composite plate structural walls [153–155]. In contrast to planar seismic force-resisting systems that are not stable out-of-plane if they are not braced, core walls are stable without lateral bracing. In the core wall system, the wall piers are typically connected by reinforced concrete coupling beams along the height of the structure [156]. The core wall system is designed in a way that the nonlinear inelastic mechanism takes place at the coupling beams and at the base of the walls, with the rest of the structure designed to remain linear elastic [156]. Similar to buildings with planar seismic force-resisting systems, the inelastic response at the core wall base reduces the first mode response. However, the higher-mode effects are not reduced by the inelastic response at the wall base [157] and they may amplify the seismic induced story shear forces and floor accelerations.

Force-limiting connections between the floors of the flexible gravity load resisting system and the stiff core wall could be used to mitigate the higher-mode effects on the dynamic response of tall buildings and contribute to the accelerated post-earthquake recovery of these buildings to a target level of functionality. However, the force-limiting connections developed for buildings with planar walls cannot be used in buildings with core walls. The reason is that the three-dimensional kinematic requirements in force-limiting connections between the floors and the core wall are different from the three-dimensional kinematic require-

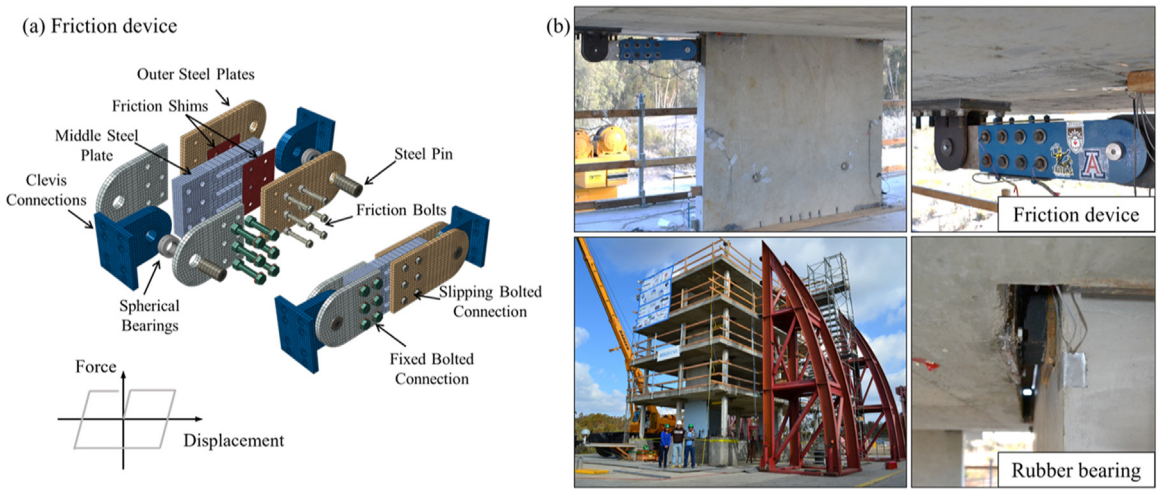



**Fig. 3.** Force-limiting connections between floors and planar seismic force-resisting systems are able to limit the contribution of higher-mode responses in the total dynamic response of the building and effectively reduce the variability in the seismic response of buildings due to the ground motion variability. (a) Friction device developed for force-limiting connections [79,87]. (b) Example of force-limiting connections in a building with planar rocking walls [79,80,88].

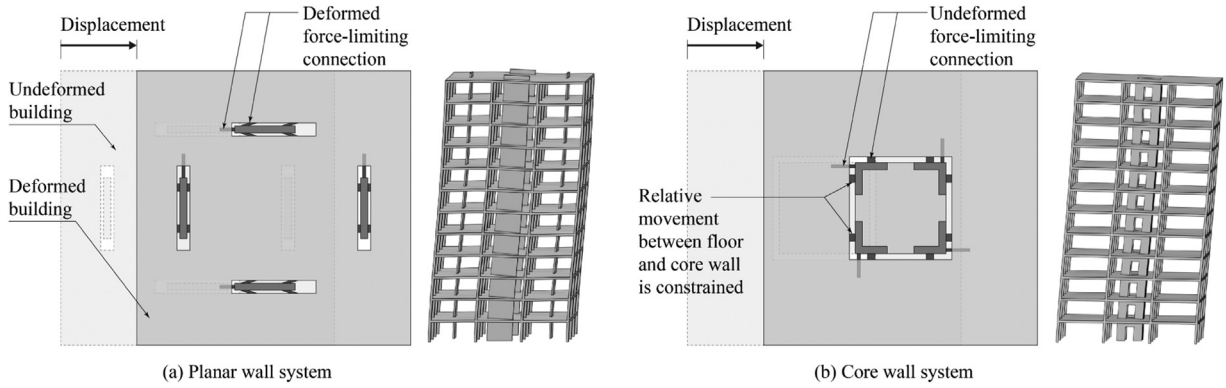



**Fig. 4.** In contrast with the planar wall system, the relative movement between the floors and the core wall system is constrained by the rubber bearings. The planar wall system is shown in (a) and the core wall system is shown in (b).

ments in force-limiting connections between floors and planar walls. The high stiffness of the rubber bearings under compression would constrain the relative movement between the floors and the core wall, making the force-limiting connection ineffective, as shown schematically in Fig. 4. In the already developed force-limiting connection for planar wall buildings, the functions of rubber bearings are (1) to provide out-of-plane stability to the planar walls and (2) to provide post-elastic stiffness to the force-limiting connection to prevent the potentially excessive connection deformation. Shake-table experimental seismic simulations of a half-scale, four-story reinforced concrete flat-plate structural wall structure with force-limiting connections conducted at the NHERI experimental facility at UC San Diego [158] showed that pounding of the slabs and the planar walls is expected at the maximum-considered-level of earthquake ground motion [80,88]. As a result, rubber bumpers are required to transfer the pounding forces. The rubber bumpers are used in addition to the friction devices and the low-damping rubber bearings. The use of conventional friction devices with constant force transferred between the floors of the flexible gravity load resisting system and the stiff core wall without the use of low-damping rubber bearings and bumpers would result in large displacement of the floor relative to the core wall and potentially uncontrolled pounding forces at the maximum-considered-level of earthquake ground motions.

Considering the above-mentioned limitations related to the use of the already developed force-limiting connections in core wall buildings, there is a need for a structural connection that can develop predetermined forces at target design displacement levels with goal to limit the force and acceleration responses of core wall buildings without inducing excessive displacement demand in the connections.

## 2. Scope of research

This paper presents a simple and practical structural connection able to develop predetermined discrete variable friction forces at target design displacement levels. As a result, a performance-based discrete variable limiting force-displacement response can be achieved. The innovative connection is termed Modified Friction Device (*Modified FD*). The term Modified FD is used to indicate that a positive effective post-elastic stiffness is achieved through the discrete variable friction force instead of the constant friction force expected in conventional friction devices. In the following sections, the schematics of the physical embodiment of the Modified FD are presented. The components and the assembly of the Modified FD are discussed. The mechanics of the Modified FD are explained. Results from static structural analyses of two types of finite element models of the Modified FD are presented. The first model is developed using solid finite elements and it is termed *Solid Model*. The Solid Model is used to assess the expected kinematics and the expected force-displacement response of the Modified FD. The second model is developed using a truss finite element and it is termed *Truss Model*. The Truss Model can be used to efficiently simulate the force-displacement response of the Modified FD in numerical earthquake simulations of

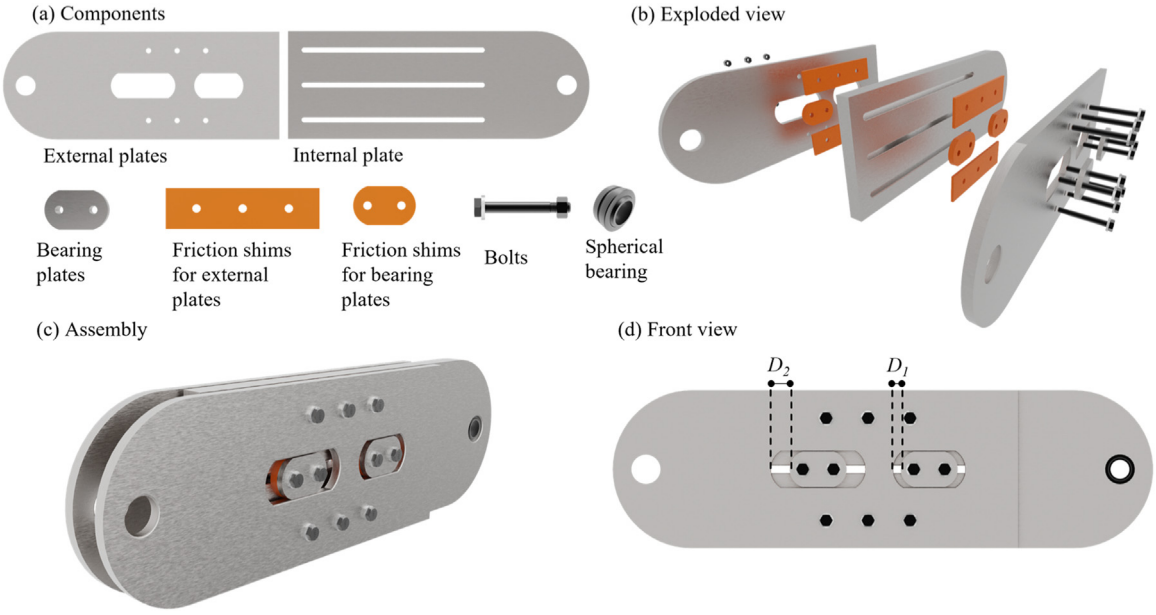



**Fig. 5.** Schematics of the Modified FD (a) components, (b) exploded view, (c) assembly, and (d) front view with initial gap dimensions $D_1$ and $D_2$ between the bearing plates and the slots in the external plates.

structural systems. The force-displacement response of the Modified FD computed using a numerical earthquake simulation of an eighteen-story reinforced concrete core wall building model is presented. The seismic response of the building model with Modified FDs is compared with the seismic response of the building model with monolithic connections and the seismic response of the building model with friction devices with constant friction forces. The results presented in this paper show that it is possible to develop a simple and practical structural connection with predetermined discrete variable force-displacement response to limit the seismic induced horizontal forces transferred between the floors of the flexible gravity load resisting system and the core wall piers in high-performance earthquake resilient buildings.

## 3. Modified FD

### 3.1. Components and assembly

Fig. 5 shows a sketch of the components, the exploded view, the assembly, and the front view of the Modified FD. The Modified FD consists of an internal plate, two external plates, four bearing plates, four friction shims between the external plates and the internal plate (termed friction shims for external plates), four friction shims between the bearing plates and the internal plate (termed friction shims for bearing plates), ten structural bolts with flat washers and nuts, and a spherical bearing. The number of bearing plates, friction shims, and bolts can be adjusted to achieve the variations of the predefined discrete variable friction force-displacement response discussed in the following sections. The end clevises used to attach a Modified FD on the floor and the seismic force-resisting system are not shown in Fig. 5. The plates and the clevises are made of structural steel ASTM A572 Grade 50. The friction shims are made of composite material similar to the laminated glass fiber fabric with graphite composite materials [159] used in friction devices developed for force-limiting connections [79].

Pretension load is applied to the bolts to clamp the external plates, the bearing plates, the friction shims, and the internal plate. The bolted components create the assembly of the Modified FD. Friction interfaces are established in the contact surfaces between the internal plate and the friction shims. The bolt load results in normal force on the friction interfaces between the friction shims and the internal plate. The friction shims for the external plates are not expected to move relative to the external plates. The friction shims for the bearing plates are not expected to move relative to the bearing plates. The slots in the internal plate allow the longitudinal motion of the friction shims, the external plates, and the bearing plates relative to the internal plate. The bearing plates and the associated friction shims are positioned within slots in the external plates, and they are not expected to move relative to the internal plate until the bearing plates are in contact with the external plates. The first gap distance between the bearing plates and the slots in the external plates is termed $D_1$, and the second gap distance between the bearing plates and the slots in the external plates is termed $D_2$, as shown in Fig. 5(d). The spherical bearings at the end of the Modified FD and the clevis allow the rotational motions and restrain the translational motions within the plane of the plates. As a result, the Modified FD is expected to develop axial load along its longitudinal direction and zero moments at the ends.

### 3.2. Expected kinematics and force-displacement response

Fig. 6 shows the expected kinematics and the expected force-displacement response of the Modified FD. The term “expected” is used because the kinematics and force-displacement response have not been validated through experimental testing. The following parameters define the expected kinematics and the expected force-displacement response: the first gap between the bearing plates and the slot in each external plate is termed $D_1$; the second gap between the bearing plates and the slot in each external plate is termed $D_2$; the friction force generated by the frictional interface between the internal plate and the friction shims for the external plates is termed $F_1$; the friction force generated by the frictional interface between the internal plate and the friction shims for the bearing plates in the slots associated with $D_1$ is termed $F_2$; the friction force generated by the frictional interface between the internal plate and the friction shims for the bearing plates in the slots associated with $D_2$ is termed $F_3$; and the elastic stiffnesses are termed $K_1$, $K_2$, and $K_3$. $K_1$ simulates the flexibility of the components of the Modified FD that are designed to have a linear elastic force-displacement response, and the shear flexibility of the friction shims associated with external plates. The linear elastic components include the clevis plates, the external plates, the internal plate, and the pins. $K_2$ and $K_3$ simulate

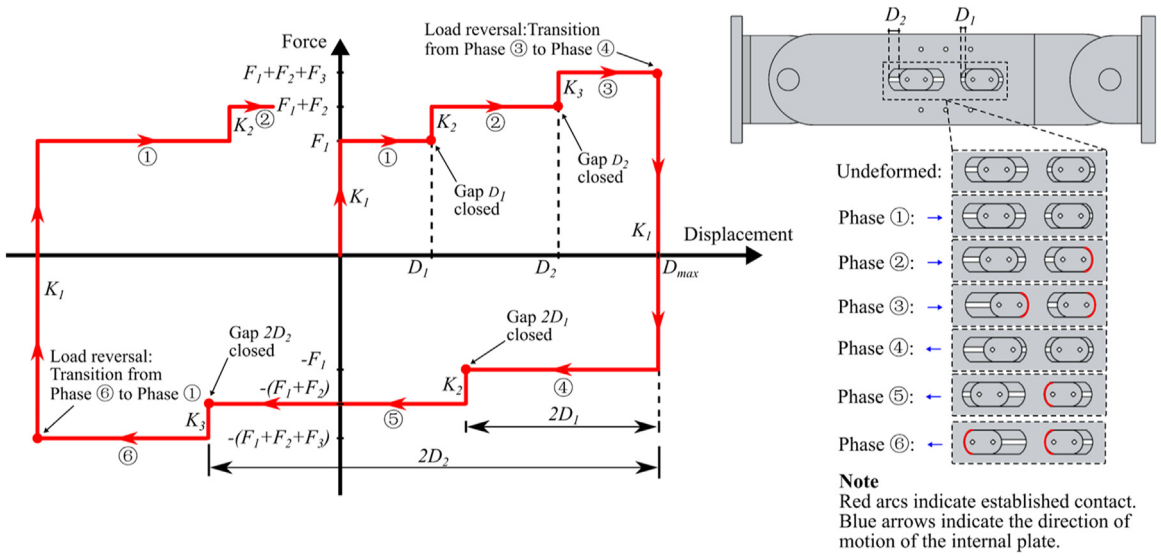



**Fig. 6.** Expected kinematics and expected force-displacement response in the Modified FD.

the flexibility of the components of the Modified FD that are designed to have a linear elastic force-displacement response, the shear flexibility of the friction shims associated with external plates, and the shear flexibility of the friction shims associated with $D_1$ and $D_2$, respectively. Six phases define the expected kinematics of the Modified FD that result in the expected force-displacement response. The expected kinematics and the expected force-displacement response described below assume that the translational motion of the external plates is restrained (i.e., pinned condition at the ends of the external plates) and that a displacement along the longitudinal direction of the Modified FD is applied at the end of the internal plates. Positive displacement results in axial tension in the Modified FD and negative displacement results in axial compression in the Modified FD. The following section presents the six phases. The discussion of the kinematics in the six phases ignores the elastic deformations $F_1/K_1$, $F_2/K_2$, and $F_3/K_3$ assuming $K_1$=$K_2$=$K_3 \cong \infty$. The rigid body kinematics of the Modified FD components are considered.

*Phase 1* – Sliding along the positive direction of motion with friction force $F_1$: The increase of the imposed displacement in the Modified FD results in increasing force with stiffness $K_1$. When the force in the Modified FD becomes equal to $F_1$, the friction shims for the external plates and the external plates start moving relative to the internal plate. The sliding at the frictional interface between the internal plate and the friction shims for the external plates results in $F_1$. $F_1$ can be estimated using Coulomb theory, $F_1 = n_s N_1 \mu_{s1}$, where $n_s = 2$ is the number of friction interfaces; $N_1$ is the total load from the six bolts acting normal to the friction interfaces between the friction shims for the external plates and the internal plate; $\mu_{s1}$ is the coefficient of friction in the friction interfaces between the friction shims for the external plates and the internal plate.

*Phase 2* – Sliding along the positive direction of motion with friction force $F_1$+$F_2$: Assuming $K_1 \cong \infty$, once the value of displacement reaches $D_1$, the external plates contact the bearing plates located in the slots associated with $D_1$. As the displacement in the Modified FD increases, the force in the Modified FD increases with stiffness $K_2$. When the force in the Modified FD becomes equal to $F_1$+$F_2$, the bearing plates and the friction shims in the slots associated with $D_1$ start moving relative to the internal plate. The sliding at the frictional interface between the internal plate and the friction shims in the slots associated with $D_1$ results in $F_2$. $F_2$ can be estimated using Coulomb theory, $F_2 = n_s N_2 \mu_{s2}$, where $N_2$ is the total load from the two bolts acting normal to the friction interfaces between the friction shims in the slots associated with $D_1$ and the internal plate; $\mu_{s2}$ is the coefficient of friction in the friction interfaces between the friction shims in the slots associated with $D_1$ and the internal plate. The total force in the Modified FD during this phase is $F_1$+$F_2$.

*Phase 3* – Sliding along the positive direction of motion with friction force $F_1$+$F_2$+$F_3$: Assuming $K_1$=$K_2 \cong \infty$, once the value of the displacement reaches $D_2$, the external plates contact the bearing plates located in the slots associated with $D_2$. As the displacement in the Modified FD increases, the force in the Modified FD increases with stiffness $K_3$. When the force in the Modified FD becomes equal to $F_1$+$F_2$+$F_3$, the bearing plates and the friction shims in the slots associated with $D_2$ start moving relative to the internal plate. The sliding at the frictional interface between the internal plate and the friction shims in the slots associated with $D_2$ results in $F_3$. $F_3$ can be estimated using Coulomb theory, $F_3 = n_s N_3 \mu_{s3}$, where $N_3$ is the total load from the two bolts acting normal to the friction interfaces between the friction shims in the slots associated with $D_2$ and the internal plate; $\mu_{s3}$ is the coefficient of friction in the friction interfaces between the friction shims in the slots associated with $D_2$ and the internal plate. The total force in the Modified FD during this phase is $F_1$+$F_2$+$F_3$. The motion continues until the Modified FD reaches the maximum imposed displacement $D_{max}$.

*Phase 4* – Sliding along the negative direction of motion with friction force -$F_1$: The reversal of the imposed displacement reduces the force in the Modified FD with elastic stiffness $K_1$. When the force in the Modified FD becomes equal to -$F_1$, the internal plate starts moving relative to the external plates along the negative direction. The friction shims for the bearing plates are not expected to move relative to the internal plate during this phase. The internal plate moves relative to the friction shims for the external plates and the external plates, resulting in a force with magnitude equal to $F_1$.

*Phase 5* – Sliding along the negative direction of motion with friction force –($F_1$+$F_2$): Assuming $K_1 \cong \infty$, once the value of displacement reaches $D_{max}$ - $2D_1$, the external plates contact the bearing plates located in the slots associated with $D_1$. As the displacement in the Modified FD decreases, the force in the Modified FD decreases with stiffness $K_2$. When the force in the Modified FD becomes equal to –($F_1$+$F_2$), the internal plate starts moving relative to the bearing plates and the friction shims in the slots associated with $D_1$. The sliding at the frictional interface between the internal

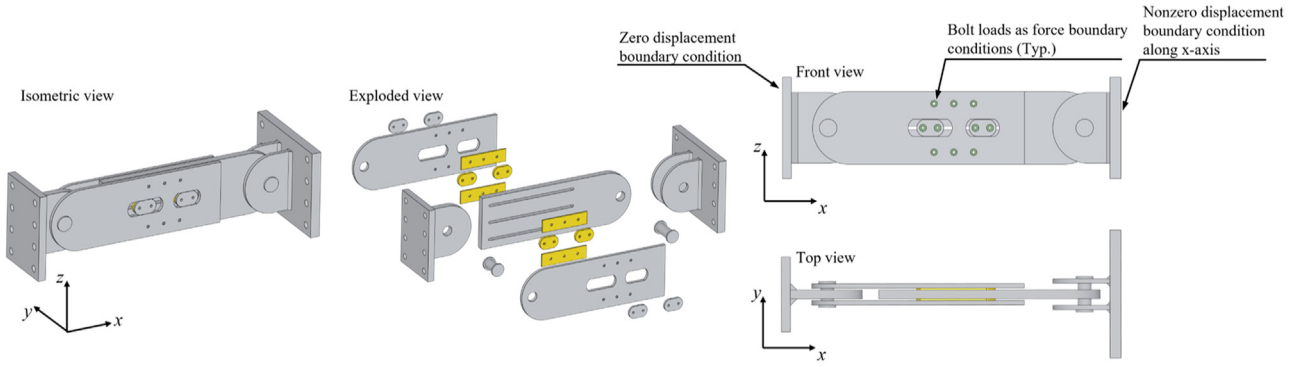



**Fig. 7.** Finite element model developed to assess the expected kinematics and the expected force-displacement response of the Modified FD.

plate and the friction shims in the slots associated with $D_1$ results in a force with magnitude equal to $F_2$. The total force in the Modified FD during this phase is $-(F_1+F_2)$.

*Phase 6* – Sliding along the negative direction of motion with friction force $-(F_1+F_2+F_3)$: Assuming $K_1 = K_2 \cong \infty$, once the value of displacement reaches $D_{max}$ - $2D_2$, the external plates contact the bearing plates located in the slots associated with $D_2$. As the displacement in the Modified FD decreases, the force in the Modified FD decreases with stiffness $K_3$. When the force in the Modified FD becomes equal to $-(F_1+F_2+F_3)$, the internal plate starts moving relative to the bearing plates and the friction shims in the slots associated with $D_2$. The sliding at the frictional interface between the internal plate and the friction shims in the slots associated with $D_2$ results in a force with magnitude equal to $F_3$. The total force in the Modified FD during this phase is $-(F_1+F_2+F_3)$.

## 4. Numerical simulations of the modified FD

Experimental characterization of the kinematics and the force-displacement response of the Modified FD is required. However, finite element analyses can be used for rapid digital prototyping of the Modified FD. For this reason, the Solid Model and the Truss Model defined in Section 2 are developed. The Solid Model is used to assess the expected kinematics and the expected force-displacement response of the Modified FD. The Truss Model is used to efficiently simulate the force-displacement response of the Modified FD in numerical earthquake simulations of structural systems. This section presents the results from the static structural analyses of the Solid Model and the Truss Model.

### 4.1. Description of the solid model

Fig. 7 shows the undeformed geometry of the Solid Model developed in ANSYS Mechanical finite element software [160] and its exploded view, front view, and top view. The Solid Model explicitly simulates the internal plate, the external plates, the bearing plates, the friction shims, the clevises, and the pins using 24,962 eight-node solid finite elements. In this model, the overall lengths (i.e., their longest dimensions along the x-direction) of the external plates are 122.56 cm, their thicknesses (i.e., their dimensions along the y-direction) are 2.54 cm and their heights (i.e., their dimensions along the z-direction) are 41.91 cm; the overall length of the internal plate is 127.64 cm, its thickness is 5.08 cm and its height is 41.91 cm; the overall lengths of the bearing plates are 15.56 cm, their thicknesses are 1.52 cm and their heights are 9.68 cm; the dimensions of the friction shims for the external plates are 38.1 cm × 1.02 cm × 10.16 cm ($x \times y \times z$); the overall lengths of the friction plates associated with the bearing plates are 15.56 cm, their thicknesses are 2.03 cm and their heights are 9.68 cm; the diameters of both pins are 7.8 cm. The bolts are assumed to be ASTM A325 structural bolts with a diameter of 19.05 mm. The minimum pretension of each bolt is 124.55 kN. ASTM A572 Grade 50 is considered for the steel plates. The Solid Model does not explicitly simulate the bolts and the associated washers and nuts used to apply the normal force on the friction interfaces. The preload of the bolts is simulated as a constant force boundary condition distributed to the nodes on the surface of the elements in the external plates and the bearing plates. The surfaces that the simulated bolt load is applied are highlighted with green color in the front view shown in Fig. 7 and they represent the common surface areas between the washers and the external plates and the common surface areas between the washers and the bearing plates. Zero displacement boundary condition is enforced at all the degrees of freedom of the nodes located on the surface of the single clevis located closer to the origin of the global x-axis. In a building application, the single clevis would have been attached to a core wall pier. As a result, the enforced boundary condition is a simplification. The simplified boundary condition is acceptable considering that the objective of the analysis of the Solid Model is to assess the expected kinematics and the expected force-displacement response of the Modified FD. For the same reason, simplified nonzero displacement boundary condition is enforced at the degrees of freedom along the global x-axis of the nodes on the surface of the double clevis further away from the origin of the global x-axis.

The Solid Model explicitly simulates the contact interfaces between the modeled components of the Modified FD using pair-based contact definition with 44,805 surface-to-surface contact elements. A contact pair is defined between each curved surface of a bearing plate and the adjacent curved surface in the slot of the external plate. These contact pairs are assumed to be frictionless. A contact pair is defined between each surface of the friction shims and the adjacent surface of the internal plate. The stress normal to the surfaces is related to the shear stress that defines the limit for the initiation of sliding using the Coulomb friction model with a constant friction coefficient equal to 0.4. The assumed friction coefficient is justified based on past experimental observations [79] of a friction device with friction interfaces established between steel and laminated glass fiber fabric with graphite composite friction shims [159]. The friction shims are assumed to be bonded on the bearing plates and the external plates. This assumption is justified considering that the bearing action of the bolts on the friction shims enforces the kinematic compatibility between the friction shims and the bearing plates and between the friction shims and the external plates. Past research has shown that it is possible to accomplish this kinematic compatibility without damaging the friction shims due to the expected bearing stresses acting on the friction shims [79]. A contact pair is defined between each surface of the pins and the surface of the internal plate where bearing is expected to occur. Similarly, a contact pair is defined between each surface of the pins and the surface of the external plates where bearing is expected to occur. A constant friction coefficient equal to 0.3 is assumed for the steel pin to steel plates contact interfaces. The components of the Modified FD are designed to remain linear elastic. All materials are simulated using a linear elastic consti-

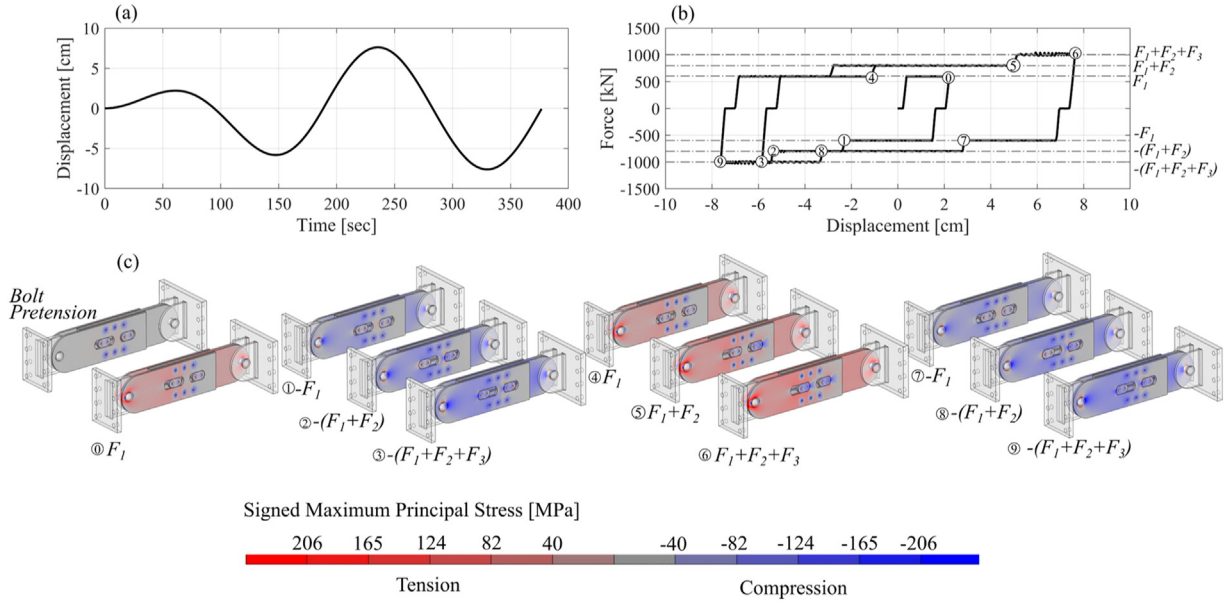



**Fig. 8.** Static structural analysis of the Solid Model shows that it is possible to develop predetermined friction forces at target design displacements with the proposed Modified FD.

tutive stress-strain relationship. The structural steel is assumed to have a modulus of elasticity equal to 200 GPa and a Poisson's ratio equal to 0.3. The composite friction material is assumed to have a modulus of elasticity equal to 6.9 GPa and a Poisson's ratio equal to 0.4.

The example parameters considered for the design of the Modified FD used to develop the Solid Model are $D_1 = 2$ cm, $D_2 = 5$ cm, $F_1 = 600$ kN, $F_2 = 200$ kN, and $F_3 = 200$ kN. The calculation of $F_1$, $F_2$, and $F_3$ follows Coulomb theory, for example, $F_1 = n_s N_1 \mu_{s1}$, where $n_s = 2$ is the number of friction interfaces; $N_1$ is the total load from the six bolts acting normal to the friction interfaces, $N_1 = 6 \times 124.55$ kN $= 747.30$ kN, given the minimum pretension of each bolt is 124.55 kN; $\mu_{s1} = 0.4$ is the assumed coefficient of friction at the friction interface. Standard oversize holes were considered for all the pin holes. As a result, the difference between the nominal diameter of the holes and the nominal diameter of the pins is equal to $\Delta_{dn} = 0.16$ cm $= 1/16$ inches. A static structural analysis of the Modified FD is performed and the stiffness matrix is updated at each converged step of analysis to account for the updated geometry. The following section shows the results from the static structural analysis of the Solid Model.

### 4.2. Solid model analysis results

Static structural analysis of the Solid Model is performed. The analysis is executed in two steps. Results from the analysis are shown in Fig. 8. The force boundary conditions that simulate the bolt pretension loads are applied in the first step of analysis. In the second step of analysis, the sinusoidal displacement shown in Fig. 8(a) is applied along the global x-axis at the degrees of freedom with the nonzero displacement boundary condition shown in Fig. 7. Fig. 8(b) shows the relationship of the applied displacement and the total reaction force along the global x-axis multiplied by −1. Positive force in the plot indicates tension in the Solid Model. The force-displacement relationship also shows the pinching displacement at zero force due to the difference between the nominal diameter of the holes and the nominal diameter of the pins. Fig. 8(c) shows the maximum principal stresses in the Solid Model at the first step of analysis and the ten sub-steps of the second step of analysis. In the first step, stresses develop in the Solid Model only due to the simulated bolt pretension. In the second step, the stress distribution at each sub-step is used to discuss the kinematics associated with the computed force-displacement response of the Solid Model. Sub-steps 0, 1, 4, and 7 are associated with force magnitude $F_1$ since contact has not been established between the bearing plates and the external plates. The gap distance $D_1$ has closed in sub-steps 2, 5, and 8. Two out of the four bearing plates are in contact with the two external plates. The increased magnitude of the maximum principal compressive stresses in the contact areas between two bearing plates and the two external plates is indicated with dark blue color as shown in Fig. 8(c). Sub-steps 2, 5, and 8 are associated with a force magnitude equal to $F_1 + F_2$. The gap distance $D_2$ has closed in sub-steps 3, 6, and 9. All bearing plates are in contact with the two external plates and high magnitude maximum principal compressive stresses are observed in the contact areas between the bearing plates and the external plates. Sub-steps 3, 6, and 9 are associated with a force magnitude equal to $F_1 + F_2 + F_3$. The simulated kinematics and the computed force-displacement relationship verify that it is possible to develop predetermined discrete variable friction forces at target design displacements with the proposed Modified FD.

### 4.3. Description of the truss model

The Truss Model simulates the force-displacement response of the Modified FD in OpenSees [161] using a corotational truss element. Fig. 9(a) shows the schematic representation of the Truss Model. A reference unit area is assigned to the truss element, termed $A_{truss}$. The length of the truss element is equal to the total approximate length of the Modified FD, termed $L_{truss}$. A uniaxial material termed *Aggregate Material* is assigned to the truss element. The term "Aggregate" is used for the uniaxial material to indicate that its stress-strain relationship is simulated by combining the stress-strain relationships of seven primary uniaxial materials. The stress of the Aggregate Material is equal to the internal force in the truss element normalized by $A_{truss}$. The strain of the Aggregate Material is equal to the axial deformation of the truss element divided by $L_{truss}$. The use of a normalized force-displacement response as the stress-strain relationship of a uniaxial material assigned to a truss element is a common modeling approach in OpenSees [78,161]. Fig. 9(b) shows the schematic representation of the combination of the seven primary uniaxial materials used to develop the Aggregate Material. The primary uniaxial materials in Fig. 9(b) are represented as springs and their normalized force-displacement behavior is defined in the following paragraphs.

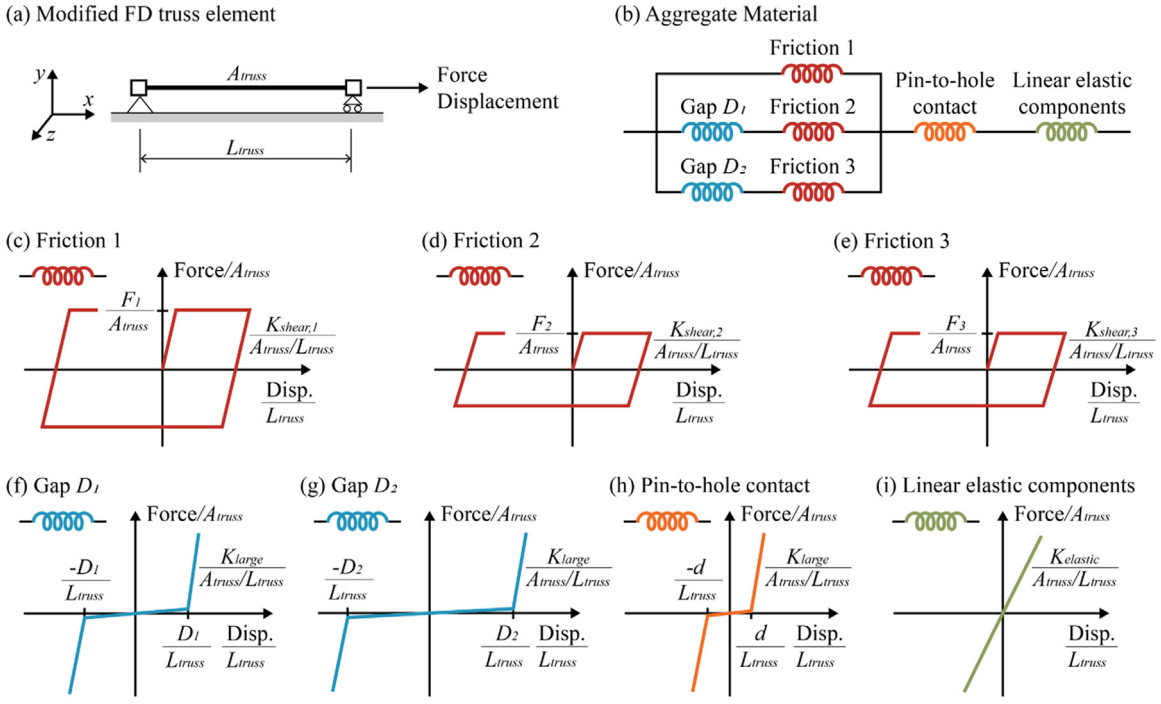



**Fig. 9.** Schematic representation of the Modified FD Truss Model and the associated material definitions.

The primary uniaxial materials termed *Friction 1, Friction 2*, and *Friction 3* simulate the normalized force-displacement behavior of the frictional interfaces that result in $F_1$, $F_2$, and $F_3$. The normalized force-displacement relationships of Friction 1, Friction 2, and Friction 3 are shown in Fig. 9(c), Fig. 9(d), and Fig. 9(e), respectively. Friction 1, Friction 2, and Friction 3 are modeled using the *Steel01* uniaxial material in OpenSees. Their normalized elastic stiffness simulates the elastic shear stiffness of the friction shims $K_{shear,i} = n_{fpi} \times G \times A_{fpi} / t_{fpi}$ normalized by $(A_{truss} / L_{truss})$. The subscript $i = 1$, 2, and 3 indicates the number associated with Friction 1, Friction 2, and Friction 3, respectively. $n_{fpi}$ is the number of friction shims associated with the development of the friction forces $F_i$. $G$ is the expected shear modulus of the material of the friction shims assuming that the same material is used for all the friction shims. $A_{fpi}$ is the surface area of the associated friction shim. $t_{fpi}$ is the thickness of the associated friction shim. Fig. 10 shows the schematic representation of the geometric terms $A_{fpi}$ and $t_{fpi}$ for $i = 1$, 2, and 3. The transition from the elastic to the post-elastic normalized force-displacement response simulates the slip between the friction shims and the internal plate associated with the friction force $F_i$ for $i = 1$, 2, and 3 normalized by $A_{truss}$.

The primary uniaxial materials, termed *Gap* $D_1$ and *Gap* $D_2$, simulate the contact behavior between the bearing plates and the external plates. They are modeled using the *ElasticMultiLinear* uniaxial material in OpenSees. The normalized force-displacement relationships of Gap $D_1$ and Gap $D_2$ are shown in Fig. 9(f) and Fig. 9(g), respectively. The pinching displacement behavior at an approximately zero normalized force is simulated with a small, normalized stiffness relative to the normalized elastic stiffness of the Modified FD. The small, normalized stiffness is assigned to the normalized force-displacement region between the normalized gap lengths $-D_j/L_{truss}$ and $D_j/L_{truss}$ where $j = 1$ or 2 indicates the gap distance $D_1$ or $D_2$, respectively. A large, normalized stiffness relative to the normalized elastic stiffness of the Modified FD is used to simulate the normalized contact stiffness between the bearing plates and the external plates.

The primary uniaxial material, termed *Pin-to-hole contact*, simulates the contact behavior between the pins and associated holes in the clevises, the external plates, and the internal plates. Fig. 9(h) shows the normalized force-displacement relationship of the *ElasticMultiLinear* uniaxial material used to simulate this contact behavior. The pinching displacement behavior at an approximately zero normalized force is simulated with a small, normalized stiffness relative to the normalized elastic stiffness of the Modified FD. The small, normalized stiffness is assigned to the normalized force-displacement region between the normalized gap lengths $-d/L_{truss} = -(4 \times \Delta_{dn})/L_{truss}$ and $d/L_{truss} = (4 \times \Delta_{dn})/L_{truss}$. A large, normalized stiffness relative to the normalized elastic stiffness of the Modified FD is used to simulate the contact stiffness between the pins, the clevises, and the plates.

The primary uniaxial material, termed *Linear Elastic Components*, simulates the flexibility of the components of the Modified FD that are designed to have a linear elastic force-displacement response. Fig. 9(i) shows the normalized force-displacement relationship of the *Elastic* uniaxial material used in OpenSees. The flexibility of the elastic components is estimated as a combination of the elastic components in series as follows:

$$1/K_{elastic} = 1/K_{CP1} + 1/K_{Pin1} + 1/K_{EPs} + 1/K_{IP} + 1/K_{Pin2} + 1/K_{CP2}$$

where $K_{CP1} = E_{steel} \times A_{CP1}/L_{CP1}$ is the estimate of the axial stiffness of the single clevis plate; $K_{\mathrm{Pin1}} = 2 \times G_{steel} \times A_{\mathrm{Pin1}}/t_{\mathrm{Pin1}}$ is the estimate of the shear stiffness of the pin connecting the external plates with the single clevis plate; $K_{EPs} = 2 \times E_{steel} \times A_{EP}/L_{EP}$ is the estimate of the axial stiffness of the two external plates; $K_{IP} = E_{steel} \times A_{IP}/L_{IP}$ is the estimate of the axial stiffness of the internal plate; $K_{\mathrm{Pin2}} = 2 \times G_{steel} \times A_{Pin2}/t_{Pin2}$ is the estimate of the shear stiffness of the pin connecting the double clevis plate with the internal plate; $K_{CP2} = 2 \times E_{steel} \times A_{\mathrm{CP2}}/L_{\mathrm{CP2}}$ is the estimate of the axial stiffness of the double clevis plate. For all the terms above, $A$, $L$, and $t$ relate to the size of components of the Modified FD and the clevis plates. Fig. 10 shows the schematic representations of the geometric terms used to compute the estimate of the stiffness of each elastic component that was considered in the computation of the flexibility of the linear elastic components. $E_{steel}$ and $G_{steel}$ are the modulus of elasticity and the shear modulus of steel, respectively. The parameters for the example Modified FD model analyzed in Section 4.1 are the following: for the structural steel, $E_{steel}$ = 200 GPa and $G_{steel}$ = 77 GPa; for the single clevis plate, $B_{CP1}$ = 40.64 cm,

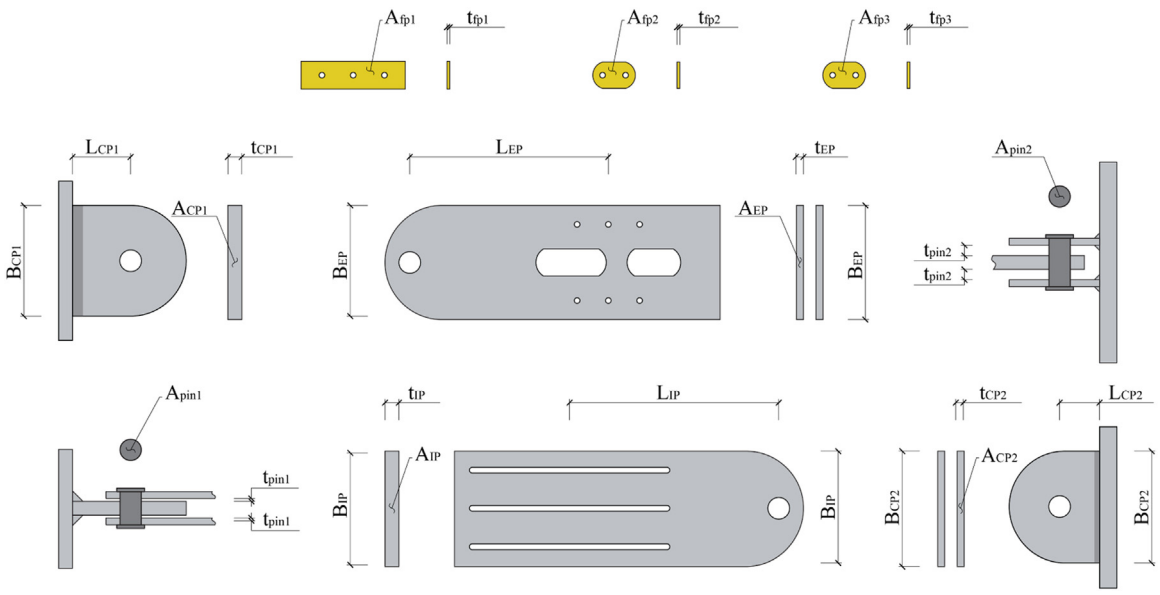



**Fig. 10.** Schematic representation of the geometric terms used to estimate the stiffness of the components of the Modified FD simulated with the Truss Model.

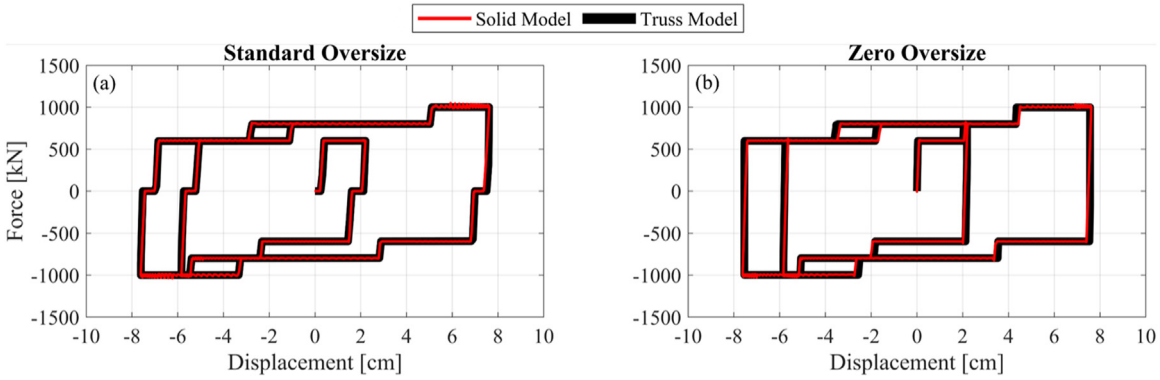



**Fig. 11.** Comparison of the force-displacement response computed using the Solid Model and the Truss Model assuming standard oversized pin holes and zero oversized pin holes.

$t_{CP1}$ = 5.08 cm, $A_{CP1} = B_{CP1} \times t_{CP1}$ = 206.45 cm$^2$ and $L_{CP1}$ = 17.46 cm; for the pin connecting the external plates with the single clevis plate, $A_{\text{Pin1}}$ = 47.78 cm$^2$ and $t_{\text{Pin1}}$ = 1.27 cm; for the external plates, $B_{EP}$ = 41.91 cm, $t_{EP}$ = 2.54 cm, $A_{EP} = B_{EP} \times t_{EP}$ = 106.45 cm$^2$ and $L_{EP}$ = 72.64 cm; for the internal plate, $B_{IP}$ = 41.91 cm, $t_{IP}$ = 5.08 cm, $A_{IP} = B_{IP} \times t_{IP}$ = 212.9 cm$^2$ and $L_{IP}$ = 72.64 cm; for the pin connecting the double clevis plate with the internal plate, $A_{\text{Pin2}}$ = 47.78 cm$^2$ and $t_{\text{Pin2}}$ = 3.81 cm; for the double clevis plate, $B_{CP2}$ = 40.64 cm, $t_{CP2}$ = 2.54 cm, $A_{CP2} = B_{CP2} \times t_{CP2}$ = 103.23 cm$^2$ and $L_{CP2}$ = 14.61 cm.

### 4.4. Truss model analysis results

Static structural analyses of the Truss Model are performed to compare the computed force-displacement response with the force-displacement response computed from the static structural analyses of the Solid Model. The axial degree of freedom at one node of the Truss Model is fixed. The displacement history shown in Fig. 8(a) is applied at the second axial degree of freedom of the Truss Model. The Truss Model assumes the design parameters considered in Section 4.1: $D_1$ = 2 cm; $D_2$ = 5 cm; $F_1$ = 600 kN; $F_2 = F_3$ = 200 kN. Fig. 11 shows results from two analysis cases. The first analysis case assumes standard oversized pin holes with a 0.16 cm = 1/16 inches difference between the diameter of the pin holes and the diameter of the pins. This analysis case is termed *Standard Oversize*. The second analysis case assumes a 0.00 cm difference between the diameter of the pin holes and the diameter of the pins. This analysis case is termed *Zero Oversize*. The Zero Oversize analysis case represents an ideal design case with machining requirements subjected to low tolerance. Low tolerance machining of the components of the Modified FD can be accomplished by using Computer Numerical Control (CNC) subtracting manufacturing methods. Fig. 11(a) and Fig. 11(b) compare the force-displacement response of the Truss Model and the force-displacement response of the Solid Model for the Standard Oversize analysis case and the Zero Oversize analysis case, respectively. The comparison of the results shows that the Truss Model approximates reasonably well the force-displacement response computed using the Solid Model. As a result, the Truss Model can be used to simulate the expected force-displacement response of the Modified FD in numerical earthquake simulations of core wall building models.

Five additional static structural analyses of the Truss Model are conducted to show the effect of the variation of the design parameters $D_1$, $D_2$, $F_1$, $F_2$, and $F_3$ in the expected force-displacement response of the Modified FD. Table 1 lists the design parameters considered in the six analysis cases discussed in this section.

The Baseline Model assumes the design parameters discussed in the Zero Oversize analysis case. DP1 assumes that the bearing plate in the slot associated with $D_1$ is replaced by a bearing plate that is 3.12 cm shorter compared to the bearing plate assumed in Baseline Model. DP2 assumes that the bearing plate in the slot associated with $D_2$ is replaced

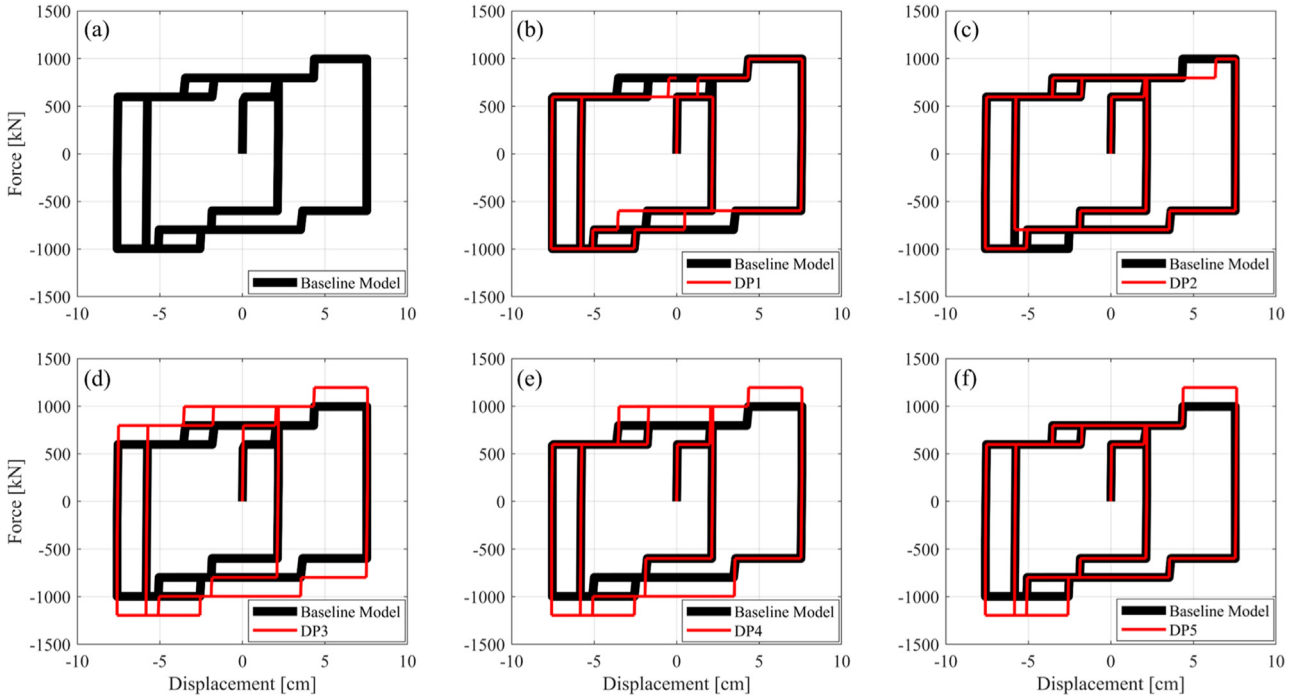



**Fig. 12.** The force-displacement responses from six analysis cases of the Truss Model show that the expected performance of the Modified FD is possible to be controlled by selecting the design parameters that lead to predefined discrete variable forces at target displacement levels.

**Table 1**
Design parameters considered in six variations of the Truss Model.

| Case of Design Parameters [-] | $D_1$ [cm] | $D_2$ [cm] | $F_1$ [kN] | $F_2$ [kN] | $F_3$ [kN] |
|---|---|---|---|---|---|
| Baseline Model | 2.00 | 5.00 | 600 | 200 | 200 |
| DP1 | 3.56 | 5.00 | 600 | 200 | 200 |
| DP2 | 2.00 | 6.35 | 600 | 200 | 200 |
| DP3 | 2.00 | 5.00 | 800 | 200 | 200 |
| DP4 | 2.00 | 5.00 | 600 | 400 | 200 |
| DP5 | 2.00 | 5.00 | 600 | 200 | 400 |

by a bearing plate that is 2.70 cm shorter compared to the bearing plate assumed in Baseline Model. DP1 and DP2 can be accomplished by replacing the associated bearing plates without revising the design of the remaining components of the Modified FD. DP3 assumes that $F_1$ is changed from 600 kN to 800 kN, which represents a case when the number of bolts contributing to $F_1$ is increased from six to eight. DP4 assumes that $F_2$ is changed from 200 kN to 400 kN, which represents a case when the number of bolts contributing to $F_2$ is increased from two to four. DP5 assumes that $F_3$ is changed from 200 kN to 400 kN, which represents a case when the number of bolts contributing to $F_3$ is increased from two to four. Static structural analyses are conducted using the displacement history shown in Fig. 8(a). Fig. 12(a) shows the force-displacement response computed from the analysis of the Baseline Model. Fig. 12(b) through (f) compare the force-displacement response of the baseline model with the force-displacement responses computed from the analysis of DP1, DP2, DP3, DP4, and DP5. The results demonstrate that the expected performance of the Modified FD is possible to be controlled by selecting the design parameters that lead to predefined forces at target displacement levels.

## 5. Seismic demands in modified FDs from numerical earthquake simulation of core wall building

In this section, the expected force and displacement seismic demands in the Modified FD are computed using results from a numerical earthquake simulation of a model of a reinforced concrete core wall building with Modified FDs. The computed displacement demands can be used as applied displacement histories in future testing for the experimental characterization of the kinematics and the force-displacement response of the Modified FD. The Modified FD between each floor and core wall pier is simulated using a Truss Model. The seismic response of the building model with Modified FDs is compared with the seismic response of the building model with monolithic connections and the seismic response of the building model with friction devices with constant friction forces. It is shown that it is possible to develop discrete variable limiting forces transferred between the floors of the flexible gravity load resisting system and the core wall piers within design target displacement levels. The detailed assessment of the seismic response of core wall buildings with Modified FD is outside the scope of this paper.

### 5.1. Numerical model of example building

An eighteen-story reinforced concrete core wall building is adopted from a reference report by Tauberg et al. (2018) [149]. The seismic force-resisting system of the building is a core wall with four L-shaped wall piers connected by coupling beams along the height of the structure, as shown in Fig. 13. The typical story height is 3.0 m (i.e., 10 ft), the length of the wall is 2.7 m (i.e., 9 ft), and the aspect ratio of the coupling beam is 3.0 with a length of 2.3 m (i.e., 7.5 ft) and a height of 0.8 m (i.e., 30 in). The slab is 0.2 m (i.e., 8 in) thick with a 1.8 m (i.e., 6 ft) cantilever slab overhang. Twelve gravity columns are located along the edge of the slab with a 9.1 m (i.e., 30 ft) distance. The structure was designed for Seismic Design Category (SDC) $D_{max}$ as defined in FEMA P695.

A three-dimensional numerical model of this eighteen-story core wall building with added Modified FDs between the floors and the core wall piers was developed in OpenSees. Fig. 14 shows the schematic representation of the eighteen-story core wall building with the Modified FDs, the numerical model of the eighteen-story core wall building, and a typical simulated floor in the numerical model of the eighteen-story core wall building. The four piers of the core wall in each story of

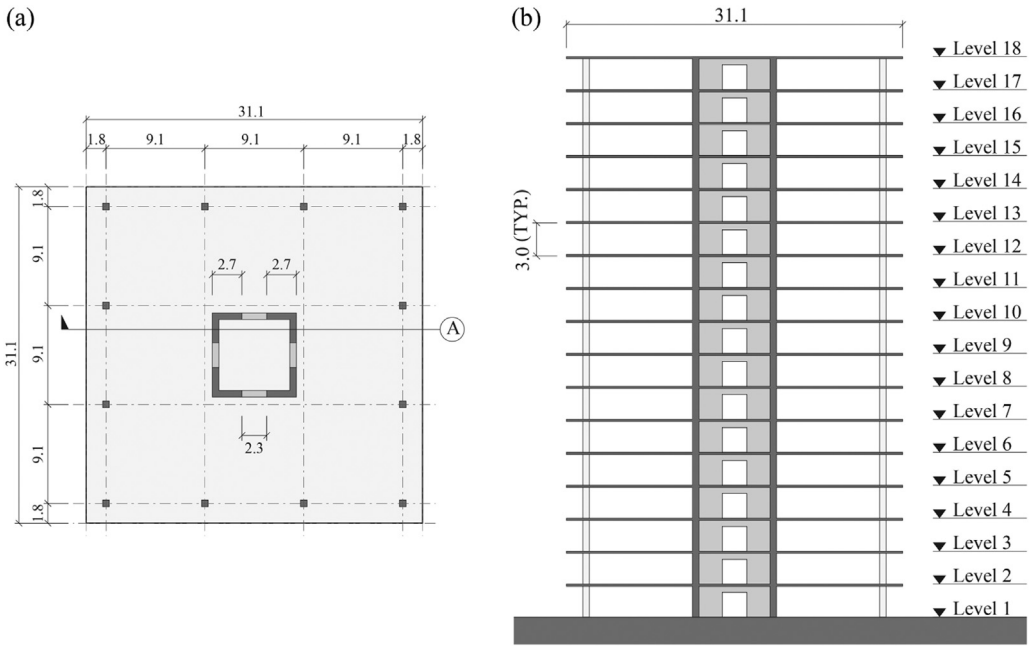



**Fig. 13.** (a) Typical floor plan and (b) section A of the eighteen-story building (all dimensions are in meters).

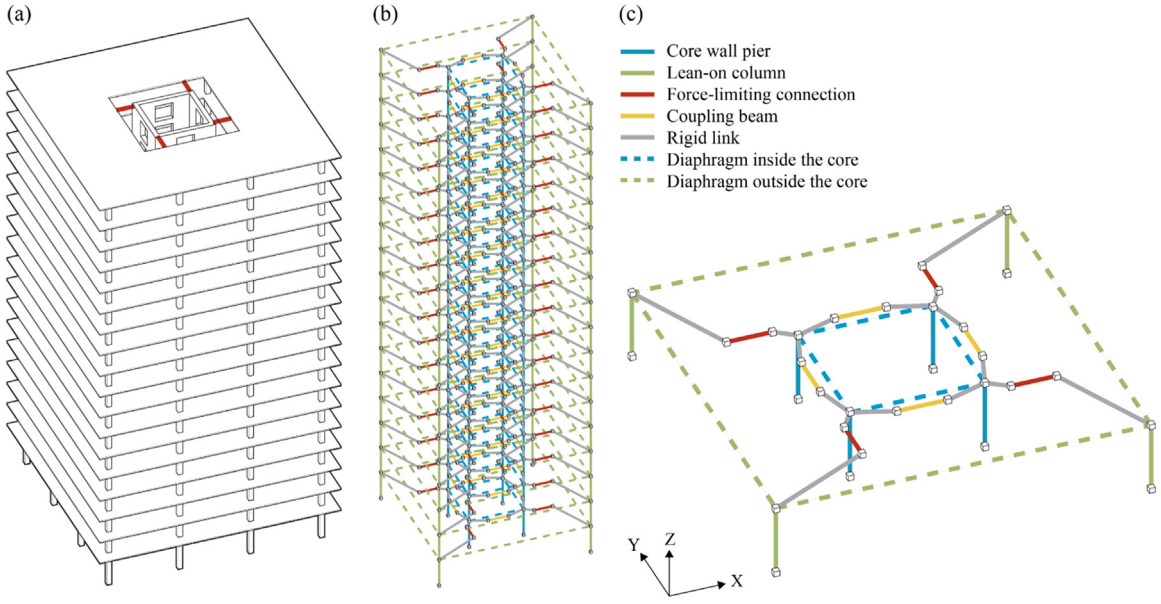



**Fig. 14.** Schematic representation of (a) the eighteen-story core wall building with the Modified FDs, (b) the numerical model of the eighteen-story core wall building and (c) a typical floor simulated in the numerical model of the building.

the building model are simulated using force-based nonlinear elements with fiber sections. The inelastic response of the coupling beams that are connecting the wall piers is simulated using lumped plasticity zero-length elements. The gravity columns are simulated using four linear elastic beam-column elements with section properties that aggregate the cracked section properties of the gravity columns. Rigid in-plane behavior is assumed for the diaphragms. The Truss Model is used to simulate the Modified FD. The Modified FD design parameters used in the model are $D_1 = 2.0$ cm, $D_2 = 5.0$ cm, and $F_2 = F_3 = 200$ kN. The values of $F_1$ on the 18th floor, 17th floor, 16th floor, 15th floor, and 1st – 14th floor are 1262 kN, 1082 kN, 902 kN, 722 kN, and 614 kN, respectively. The values of $F_1$ at each floor were computed using a force-based method proposed by Tsampras and Sause (2022) [81]. This method is modified from the ASCE/SEI 7–16 [162] alternative seismic design force method for floor diaphragms. Numerical earthquake simulations [81] demonstrated that using this method in designing reinforced concrete planar wall buildings with force-limiting connections would result in reasonable connection deformation demands and relatively uniform distribution connection deformation demands over the height of the building.

The building model was subjected to a ground motion recorded at Shin-Osaka station during the 1995 earthquake in Kobe, Japan, scaled to the design level of the expected earthquake ground motion. The two horizontal components of the scaled ground acceleration, SHI000 (H1) and SHI090 (H2), are shown in Fig. 15(a) and Fig. 15(b), respectively. Fig. 15(c) shows the response spectra of the scaled ground motion and the design spectrum with a 5% damping ratio. The natural periods of the first, second, and third translational modes of the building model properties are also plotted in Fig. 15(c). H1 and H2 are applied at

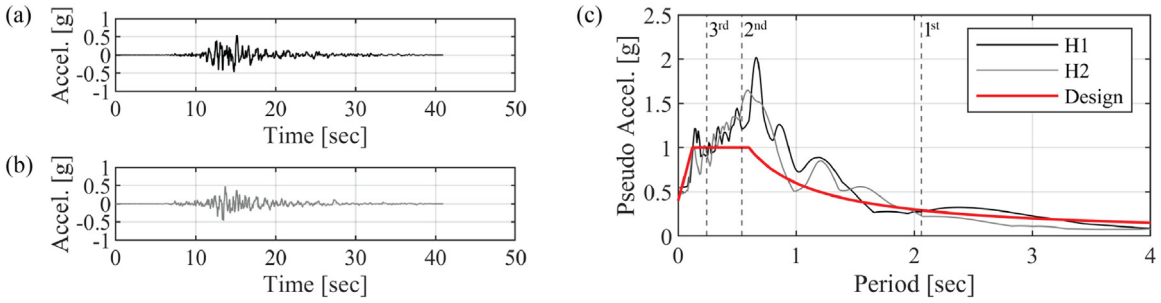



**Fig. 15.** Scaled ground acceleration of the two horizontal components (a) SHI000 (H1) and (b) SHI090 (H2), and (c) pseudo acceleration response spectra of scaled ground motions and design spectrum with a 5% damping ratio. The dashed lines are associated with the natural periods of the first, second, and third translational modes of the building model.

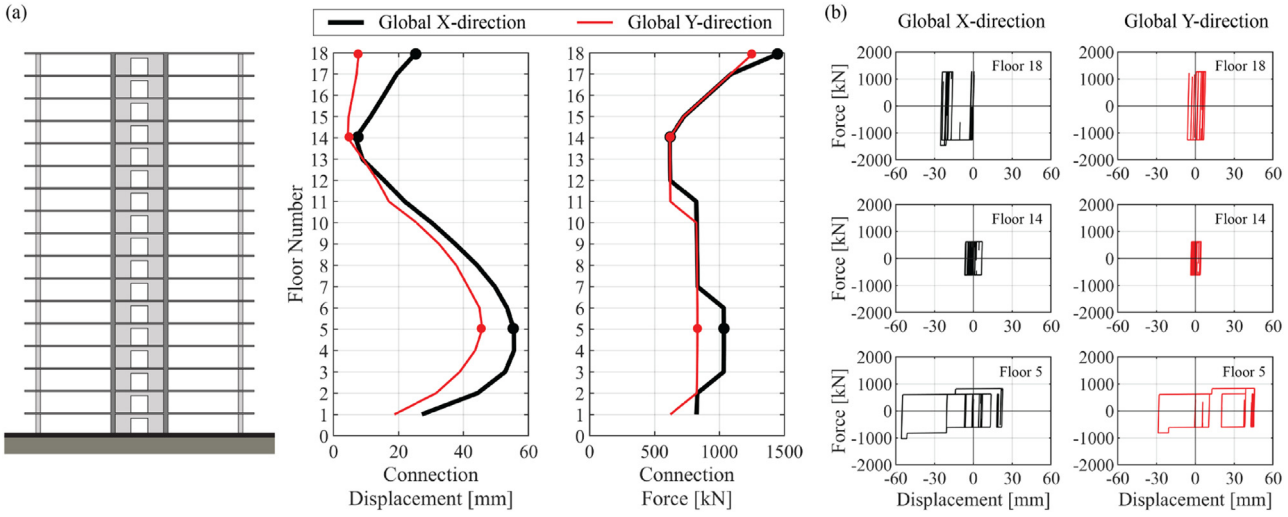



**Fig. 16.** Peak force and peak displacement responses in the Modified FD along the global X- and Y-directions, and (b) the force-displacement response of the Modified FD at floor levels 5, 14, and 18.

the base of the building model along the global X- and Y- directions, respectively.

### 5.2. *Seismic response of the modified FD in the example building model*

Fig. 16 shows the force and displacement seismic responses of the Modified FD computed using analysis results from the numerical earthquake simulation. Fig. 16(a) shows the peak (i.e., absolute maximum) response of the Modified FD connection displacement and connection forces over the height of the building model. The peak responses are computed at each floor level. The black lines are associated with the peak responses in the global X-direction, and the red lines are associated with the peak responses in the global Y-direction. The peak connection forces show the activation of different force levels at different floors to limit the displacement demand. For example, due to the contribution of the second and higher translational mode responses in the total dynamic response of the building, the peak connection deformation is the largest near floor levels from 3 to 6, and larger connection forces are activated at the corresponding floor levels to limit the large displacement demand. Fig. 16(b) shows the force-displacement responses of the Modified FD at floor levels 5, 14, and 18, representing the largest response, the smallest response, and the response at the roof, respectively. On the 5th floor, the connection force reached $F_1+F_2+F_3$ and $F_1+F_2$ in the global X- and Y-directions, respectively. On the 14th floor, where the deformation is the smallest, only the connection force $F_1$ was activated in both the global X- and Y-directions. On the 18th floor, the connection force reached $F_1+F_2$ and $F_1$ in the global X- and Y-directions, respectively. The numerical earthquake simulation results show that it is possible to limit the forces transferred from the floors to the core wall piers in a controlled manner through the expected predetermined discrete variable force-displacement response of the Modified FD simulated using the Truss Model.

The seismic responses of the eighteen-story reinforced concrete core wall building model with three types of connections are compared. The first type of connection assumes conventional monolithic connections between the floors and the core wall system; the second type of connection assumes the use of friction devices with constant friction forces, termed FD; the third type of connection assumes the use of Modified FDs. The monolithic connections are simulated using a linear-elastic force-displacement response with high elastic stiffness to approximate a rigid behavior. The FDs are simulated using elastic-perfectly plastic force-displacement response (i.e., zero post-elastic stiffness). The elastic stiffness of the FDs is equal to the elastic stiffness of the Modified FDs. The post-elastic force of the FDs is equal to $F_1$ discussed in Section 5.1. Fig. 17 shows the peak floor total acceleration, the peak connection displacement, and the peak connection force in global X- and Y-directions over the height of the building model. The use of FDs or Modified FDs reduces the peak floor total acceleration and the peak connection force compared to the use of monolithic connections. In addition to the reduction of acceleration and force responses, the use of Modified FDs effectively reduces the peak connection displacement compared to the use of FDs. The peak connection displacement of the monolithic connections is close to zero due to the high connection stiffness.

The numerical earthquake simulation results showed that the use of the Modified FDs can limit the seismic induced horizontal forces transferred from the floors to the core wall of the example building model

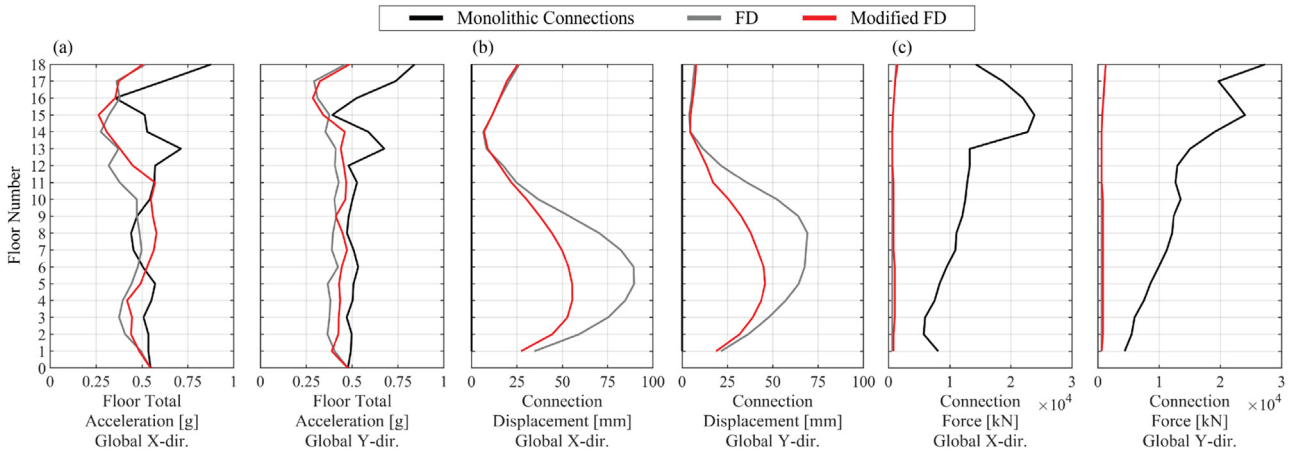



**Fig. 17.** Peak floor total acceleration, peak connection displacement, and peak connection force in global X- and Y-directions.

without inducing excessive connection displacement demand. Further research is required to determine the effect of the characteristics of earthquake strong ground motions in the seismic response of multistory reinforced concrete core wall buildings with Modified FDs and to determine the values of the design parameters of the Modified FD that result in target seismic performance of core wall buildings.

## 6. Conclusions

A simple and practical structural connection that develops predetermined discrete variable friction forces at target design displacement levels was presented. The innovative connection was termed Modified Friction Device (Modified FD). Modified FDs are used to transfer the seismic induced horizontal forces from the floors to the core wall seismic force-resisting system of a building. The schematics of the physical embodiment of the Modified FD were presented. The components and the assembly of the Modified FD were discussed. The mechanics of the Modified FD were explained. Results from numerical simulations of a solid finite element model of the Modified FD validated the expected kinematics and the expected force-displacement response of the Modified FD. A truss finite element model was developed in OpenSees. It was shown that the truss model simulates efficiently and reasonably well the expected force-displacement response of the Modified FD. Numerical earthquake simulations of an eighteen-story reinforced concrete core wall building model with three types of connections (i.e., conventional monolithic connections, friction devices with constant friction forces, and the Modified FD) were conducted using OpenSees. The numerical earthquake simulation results showed that the use of the Modified FDs can limit the seismic induced horizontal forces transferred from the floors to the core wall of the example building model without inducing excessive connection displacement demand.

Further research is required to determine the effect of the characteristics of earthquake strong ground motions in the seismic response of multistory reinforced concrete core wall buildings with Modified FDs and to determine the values of the design parameters of the Modified FD that result in target seismic performance of core wall buildings. Experimental characterization of the kinematics and the force-displacement response of the Modified FD is required.

## Declaration of Competing Interest

The authors declare that they have no known competing financial interests or personal relationships that could have appeared to influence the work reported in this paper.

## Acknowledgments

The authors are grateful for financial support provided by Structural Engineering Distinguished Fellowship and additional support from the Department of Structural Engineering at UC San Diego. Any opinions, findings, and conclusions expressed in this paper are those of the authors and do not necessarily reflect the views of the party acknowledged here.

## References

[1] Guha-Sapir D., Below R., Hoyois P. EM-DAT | The international disasters database 2022. https://www.emdat.be/ (accessed February 7, 2022).
[2] Wikipedia. 2011 Christchurch earthquake. 2022.
[3] Tsampras G. Force-limiting floor diaphragm connection for earthquake-resistant buildings. PhD. Lehigh University, 2016.
[4] Google Books Ngram Viewer 2022. https://books.google.com/ngrams/info (accessed February 7, 2022).
[5] California demographics https://www.dof.ca.gov/Forecasting/Demographics/(accessed February 7, 2022).
[6] Congressional Research Service. The national earthquake hazards reduction program (NEHRP): issues in brief. Washington, D.C.: 2021.
[7] FEMA. NEHRP recommended seismic provisions for new buildings and other structures. FEMA; 2020.
[8] National Research Council National earthquake resilience: research, implementation, and outreach. Washington, DC: National Academies Press; 2011. doi:1017226/13092.
[9] McAllister TP, Walker R, Baker A. Assessment of resilience in codes, standards, regulations, and best practices for buildings and infrastructure systems. Gaithersburg, MD: National Institute of Standards and Technology; 2022.
[10] Building Seismic Safety Council Issues and research needs identified during development of the 2015 nehrp recommended seismic provisions for new buildings and other structures. Washington, DC: National Institute of Building Sciences; 2015.
[11] FEMA. Recommended future issues and research needs identified during the development of the 2020 NEHRP recommended seismic provisions for new buildings and other structures. 2021.
[12] FEMA Guidelines for nonlinear structural analysis and design of buildings. part i - general. Gaithersburg, MD: National Institute of Standards and Technology; 2017. doi:106028/NISTGCR17-917-46v1.
[13] FEMA Seismic performance assessment of buildings, volume 1 – Methodology. Second Edition. Federal Emergency Management Agency; 2018.
[14] Segura C, Sattar S. Uncertainty in the seismic response of reinforced concrete structures due to material variability. In: Proceedings of the 17th World Conference on Earthquake Engineering; 2020.
[15] Moehle JP, Hooper JD, Kelly DJ, Meyer TR. Seismic design of cast-in-place concrete diaphragms, chords, and collectors. National Institute of Standards and Technology; 2010.
[16] Fleischman RB, Farrow KT. Dynamic behavior of perimeter lateral-system structures with flexible diaphragms. Earthq Eng Struct Dyn 2001;30:745–63. doi:10.1002/eqe.36.
[17] Rodriguez ME, Restrepo JI, Carr AJ. Earthquake-induced floor horizontal accelerations in buildings. Earthq Eng Struct Dyn 2002;31:693–718. doi:10.1002/eqe.149.
[18] Rodriguez ME, Restrepo JI, Blandón JJ. Seismic design forces for rigid floor diaphragms in precast concrete building structures. J Struct Eng 2007;133:1604–15. doi:10.1061/(ASCE)0733-9445(2007)133:11(1604).
[19] Fleischman RB, Restrepo JI, Naito CJ, Sause R, Zhang D, Schoettler M. Integrated analytical and experimental research to develop a new seismic design methodology for precast concrete diaphragms. J Struct Eng 2013;139:1192–204. doi:10.1061/(ASCE)ST.1943-541X.0000734.

[20] Iverson JK, Hawkins NM. Performance of precast/prestressed concrete building structures during northridge earthquake. PCI J 1994:39.
[21] Tilt-up-wall buildings. Earthq Spectra 1996;12:99–123. doi:10.1193/1.1585922.
[22] Gonzalez A, Spacone E, Nascimbene R. Performance-based seismic design framework for RC floor diaphragms in dual systems. Procedia Eng 2017;199:3546–51. doi:10.1016/j.proeng.2017.09.512.
[23] Scarry J.M. Floor diaphragms – Seismic bulwark or Achilles' heel. NZSEE Conference, 2014.
[24] Kam W.Y., Pampanin S., Elwood K. Seismic performance of reinforced concrete buildings in the 22 February Christchurch (Lyttleton) earthquake 2011.
[25] Bruneau M., MacRae G. Reconstructing Christchurch: a seismic shift in building structural systems. Quake Core; 2017.
[26] Uang C-M, Bruneau M. State-of-the-art review on seismic design of steel structures. J Struct Eng 2018;144:03118002. doi:10.1061/(ASCE)ST.1943-541X.0001973.
[27] Kelly JM, Skinner RI, Heine AJ. Mechanisms of energy absorption in special devices for use in earthquake resistant structures. Bull N Z Soc Earthq Eng 1972;5.
[28] Kelly JM, Tsztoo DF. Earthquake simulation testing of a stepping frame with energy-absorbing devices. Bull N Z Soc Earthq Eng 1977;10:196–207. doi:10.5459/bnzsee.10.4.196-207.
[29] Priestley MJN, MacRae GA. Seismic tests of precast beam-to-column joint subassemblages with unbonded tendons. PCI J 1996;41:64–81. doi:10.15554/pcij.01011996.64.81.
[30] Priestley MJN, Sritharan S, Conley JR, Stefano Pampanin S. Preliminary results and conclusions from the PRESSS five-story precast concrete test building. PCI J 1999;44:42–67. doi:10.15554/pcij.11011999.42.67.
[31] Christopoulos C, Filiatrault A, Uang CM, Folz B. Posttensioned energy dissipating connections for moment-resisting steel frames. J Struct Eng 2002;128:1111–20. doi:10.1061/(ASCE)0733-9445(2002)128:9(1111).
[32] Ricles JM, Sause R, Garlock MM, Zhao C. Posttensioned seismic-resistant connections for steel frames. J Struct Eng 2001;127:113–21. doi:10.1061/(ASCE)0733-9445(2001)127:2(113).
[33] Rojas P, Ricles JM, Sause R. Seismic performance of post-tensioned steel moment resisting frames with friction devices. J Struct Eng 2005;131:529–40. doi:10.1061/(ASCE)0733-9445(2005)131:4(529).
[34] Granello G, Palermo A, Pampanin S, Pei S, van de Lindt J. Preslam buildings: state-of-the-art. J Struct Eng 2020;146:04020085. doi:10.1061/(ASCE)ST.1943-541X.0002603.
[35] Perez F de J. Lateral load behavior and design of unbonded post-tensioned precast concrete walls with ductile vertical joint connectors. Precast/Prestressed Concrete Institute; 1998. 10.15554/pci.rr.seis-018.
[36] Kurama Y., Sause R., Pessiki S., Lu L.W. Lateral load behavior and seismic design of unbonded post-tensioned precast concrete walls. SJ 1999;96:622–32. 10.14359/700.
[37] Kurama Y.C. Simplified seismic design approach for friction-damped unbonded post-tensioned precast concrete walls. SJ 2001;98:705–16. 10.14359/10624.
[38] Perez FJ, Pessiki S, Sause R. Lateral load behavior of unbonded post-tensioned precast concrete walls with vertical joints. PCI J 2004;49:48–64. doi:10.15554/pcij.03012004.48.64.
[39] Restrepo JI, Rahman A. Seismic performance of self-centering structural walls incorporating energy dissipators. J Struct Eng 2007;133:1560–70. doi:10.1061/(ASCE)0733-9445(2007)133:11(1560).
[40] Holden T, Restrepo J, Mander JB. Seismic performance of precast reinforced and prestressed concrete walls. J Struct Eng 2003;129:286–96. doi:10.1061/(ASCE)0733-9445(2003)129:3(286).
[41] Ajrab JJ, Pekcan G, Mander JB. Rocking wall–frame structures with supplemental tendon systems. J Struct Eng 2004;130:895–903. doi:10.1061/(ASCE)0733-9445(2004)130:6(895).
[42] Meek JW. Dynamic response of tipping core buildings. Earthq Eng Struct Dyn 1978;6:437–54. doi:10.1002/eqe.4290060503.
[43] Ganey R, Berman J, Akbas T, Loftus S, Daniel Dolan J, Sause R, et al. Experimental investigation of self-centering cross-laminated timber walls. J Struct Eng 2017;143:04017135. doi:10.1061/(ASCE)ST.1943-541X.0001877.
[44] Buchanan A, Deam B, Fragiacomo M, Pampanin S, Palermo A. Multi-storey prestressed timber buildings in New Zealand. Struct Eng Int 2008;18:166–73. doi:10.2749/101686608784218635.
[45] Makris N, Aghagholizadeh M. Effect of supplemental hysteretic and viscous damping on rocking response of free-standing columns. J Eng Mech 2019;145:04019028. doi:10.1061/(ASCE)EM.1943-7889.0001596.
[46] Roke D. Damage-free seismic-resistant self-centering concentrically-braced frames. PhD. Lehigh University, 2010.
[47] Sause R, Ricles JM, Roke DA, Chancellor NB, Gonner NP. Large-scale experimental studies of damage-free self-centering concentrically-braced frame under seismic loading. In: Proceedings of the structures congress 2010; 2010. p. 1498–509. : American Society of Civil Engineers. doi:10.1061/41130(369)136.
[48] Deierlein G, Krawinkler H, Ma X, Eatherton M, Hajjar J, Takeuchi T, et al. Earthquake resilient steel braced frames with controlled rocking and energy dissipating fuses. Steel Constr 2011;4:171–5. doi:10.1002/stco.201110023.
[49] Ma X., Krawinkler H., Deierlein G.G. Seismic design and behavior of self-centering braced frame with controlled rocking and energy dissipating fuses. John A. Blume Earthquake Engineering Center Department of Civil and Environmental Engineering; 2011.
[50] Eatherton M, Hajjar J, Ma X, Krawinkler H, Deierlein G. Seismic design and behavior of steel frames with controlled rocking—part i: concepts and quasi-static subassembly testing. In: Proceedings of the ASCE structures congress 2010; 2012. p. 1523–33. : American Society of Civil Engineers. doi:10.1061/41130(369)138.
[51] Martin A, Deierlein GG. Generalized modified modal superposition procedure for seismic design of rocking and pivoting steel spine systems. J Constr Steel Res 2021;183:106745. doi:10.1016/j.jcsr.2021.106745.
[52] Christopoulos C, Zhong C. Towards understanding, estimating and mitigating higher-mode effects for more resilient tall buildings. Resilient Cities Struct 2022;1:53–64. doi:10.1016/j.rcns.2022.03.005.
[53] Pampanin S, Vacareanu R, Ionescu C. NextGen building systems - S4: seismically safer, sustainable and smart - raising the bar to enhance community resilience and sustainability. In: Progresses in european earthquake engineering and seismology. Cham: Springer International Publishing; 2022. p. 343–62. doi:10.1007/978-3-031-15104-0_21.
[54] Bianchi S, Ciurlanti J, Perrone D, Filiatrault A, Costa AC, Candeias PX, et al. Shake-table tests of innovative drift sensitive nonstructural elements in a low-damage structural system. Earthq Eng Struct Dyn 2020. doi:10.1002/eqe.3452.
[55] Zhong C, Christopoulos C. Self-centering seismic-resistant structures: historical overview and state-of-the-art. Earthq Spectra 2021 87552930211057580. doi:10.1177/87552930211057581.
[56] Alavi B, Krawinkler H. Strengthening of moment-resisting frame structures against near-fault ground motion effects. Earthq Eng Struct Dyn 2004;33:707–22. doi:10.1002/eqe.370.
[57] Mar D. Design examples using mode shaping spines for frame and wall buildings. In: Proceedings of the 9th U.S. National and 10th Canadian conference on earthquake engineering, Toronto, Ontario; 2010.
[58] Wada A, Qu Z, Motoyui S, Sakata H. Seismic retrofit of existing SRC frames using rocking walls and steel dampers. Front Archit Civ Eng China 2011;5:259. doi:10.1007/s11709-011-0114-x.
[59] Qu Z, Wada A, Motoyui S, Sakata H, Kishiki S. Pin-supported walls for enhancing the seismic performance of building structures. Earthq Eng Struct Dyn 2012;41:2075–91. doi:10.1002/eqe.2175.
[60] Janhunen B, Tipping S, Wolfe J. Seismic retrofit of a 1960s steel moment-frame highrise using a pivoting spine. In: Proceedings of the SEAOC 2013 Convention; 2013.
[61] Lai JW, Mahin SA. Strongback system: a way to reduce damage concentration in steel-braced frames. J Struct Eng 2015;141:04014223. doi:10.1061/(ASCE)ST.1943-541X.0001198.
[62] Chen X, Takeuchi T, Matsui R. Seismic performance and evaluation of controlled spine frames applied in high-rise buildings. Earthq Spectra 2018;34:1431–58. doi:10.1193/080817EQS157M.
[63] Simpson BG, Mahin SA. Experimental and numerical investigation of strongback braced frame system to mitigate weak story behavior. J Struct Eng 2018;144:04017211. doi:10.1061/(ASCE)ST.1943-541X.0001960.
[64] Osteraas J., Hunt J., Luth G., Luth G.P., Clara S. Performance based seismic design of the gigafactory in Tesla Time 2017:13.
[65] Simpson B. Design development for steel strongback braced frames to mitigate concentrations of damage. PhD. UC Berkeley, 2018.
[66] Fahnestock L, Sause R, Ricles J, Simpson B, Kurata M, Okazaki T, et al. U.S.-Japan collaboration for shake table testing of a frame-spine system with force-limiting connections. In: Proceedings of the 17th world conference on earthquake engineering; 2021.
[67] Fahnestock L, Sause R, Ricles J, Simpson B, Kurata M, Okazaki T, et al. Frame-spine system with force-limiting connections for low-damage seismic-resilient buildings. In: Proceedings of the 10th international conference on behaviour of steel structures in seismic areas. Cham: Springer International Publishing; 2022. p. 804–11. doi:10.1007/978-3-031-03811-2_88.
[68] Kelly E. Floor response of yielding structures. Bull N Z Soc Earthq Eng 1978:18.
[69] Flores FX, Lopez-Garcia D, Charney FA. Assessment of floor accelerations in special steel moment frames. J Constr Steel Res 2015;106:154–65. doi:10.1016/j.jcsr.2014.12.006.
[70] Sewell R, Cornell C, Toro G, McGuire R. A study of factors influencing floor response spectra in nonlinear multi-degree-of-freedom structures. USA: Stanford University; 1986.
[71] Chopra AK. Dynamics of structures. Pearson Education; 2007.
[72] Priestley MJ, Amaris AD. Dynamic amplification of seismic moments and shear forces in cantilever walls. IUSS Press; 2002.
[73] Wiebe L, Christopoulos C. Mitigation of higher mode effects in base-rocking systems by using multiple rocking sections. J Earthq Eng 2009;13:83–108. doi:10.1080/13632460902813315.
[74] Wiebe L, Christopoulos C, Tremblay R, Leclerc M. Mechanisms to limit higher mode effects in a controlled rocking steel frame. 1: concept, modelling, and low-amplitude shake table testing: mechanisms to limit higher mode effects: concept, low-amplitude tests. Earthq Eng Struct Dyn 2013;42:1053–68. doi:10.1002/eqe.2259.
[75] Panagiotou M, Restrepo JI. Dual-plastic hinge design concept for reducing higher-mode effects on high-rise cantilever wall buildings. Earthq Eng Struct Dyn 2009;38:1359–80. doi:10.1002/eqe.905.
[76] Zhang D, Fleischman R, Restrepo J, Sause R, Maffei J, Mar D, et al. Development of a floor inertial force limiting anchorage system building seismic response. In: Proceedings of the 10th U.S. National conference on earthquake engineering; 2014. p. 11. 10th U.S. National Conference on Earthquake Engineering.
[77] Tsampras G, Sause R, Zhang D, Fleischman RB, Restrepo JI, Mar D, et al. Development of deformable connection for earthquake-resistant buildings to reduce floor accelerations and force responses. Earthq Eng Struct Dyn 2016;45:1473–94. doi:10.1002/eqe.2718.
[78] Tsampras G, Sause R, Fleischman RB, Restrepo JI. Experimental study of deformable connection consisting of buckling-restrained brace and rubber bearings to connect floor system to lateral force resisting system. Earthq Eng Struct Dyn 2017;46:1287–305. doi:10.1002/eqe.2856.

[79] Tsampras G, Sause R, Fleischman RB, Restrepo JI. Experimental study of deformable connection consisting of friction device and rubber bearings to connect floor system to lateral force resisting system. Earthq Eng Struct Dyn 2018;47:1032–53. doi:10.1002/eqe.3004.
[80] Zhang Z, Fleischman RB, Restrepo JI, Guerrini G, Nema A, Zhang D, et al. Shake-table test performance of an inertial force-limiting floor anchorage system. Earthq Eng Struct Dyn 2018;47:1987–2011. doi:10.1002/eqe.3047.
[81] Tsampras G, Sause R. Force-based design method for force-limiting deformable connections in earthquake-resistant buildings. J Struct Eng 2022;148. doi:10.1061/(ASCE)ST.1943-541X.0003456.
[82] Nema A. Development of low seismic damage structural systems. PhD. UC San Diego, 2018.
[83] Zhang Z. Analytical investigation of inertial force-limiting floor anchorage system for seismic resistant building structures. PhD. The University of Arizona, 2017.
[84] Tsampras G, Sause R, Fleischman RB, Restrepo JI, Nema A, Zhang Z. Practical force-limiting deformable connections in buildings with rocking base mechanism and limited higher-mode responses. In: Proceedings of the 12th national conference on earthquake engineering. Salt Lake City, Utah: EERI; 2022.
[85] Paronesso M, Lignos DG. Seismic design and performance of steel concentrically braced frame buildings with dissipative floor connectors. Earthq Eng Struct Dyn 2022;51:3505–25. doi:10.1002/eqe.3733.
[86] Paronesso M, Lignos DG. Experimental study of sliding friction damper with composite materials for earthquake resistant structures. Eng Struct 2021;248:113063. doi:10.1016/j.engstruct.2021.113063.
[87] Tsampras G., Sause R. Full-scale, components test of inertial force-limiting floor anchorage systems for seismic resistant building structures using a friction device and carbon fiber reinforced low damping rubber bearings. DesignSafe-CI; 2014.
[88] Fleischman R.B., Restrepo J.I., Sause R., Zhang D., Tsampras G., Zhang Z., et al. Half scale shake table test of a 4 story reinforced concrete building with eccentric Shear walls. DesignSafe-CI; 2014.
[89] Clark P, Bassett R, Bradshaw J. Plate friction load control devices - Their application and potential. Proc Inst Civ Eng 1973;55:335–52.
[90] Loo Y, Upfold R. The behavior of an earthquake energy absorber for bridge decks. In: Proceedings of the sixth Australian conference on the mechanics of structures and materials. University of Canterbury; 1977. p. 365–71.
[91] Pall A.S. Limited slip bolted joints : a device to control the seismic response of large panel structures. PhD. Concordia University, 1979.
[92] Bora C, Oliva MG, Nakaki SD, Becker R. Development of a precast concrete shear-wall system requiring special code acceptance. PCI J 2007;52:122–35. doi:10.15554/pcij.01012007.122.135.
[93] Morgen BG. Friction-Damped unbonded post-tensioned precast concrete moment frame structures for seismic regions. University Of Notre Dame; 2007.
[94] Morgen BG, Kurama YC. Seismic response evaluation of posttensioned precast concrete frames with friction dampers. J Struct Eng 2008;134:132–45. doi:10.1061/(ASCE)0733-9445(2008)134:1(132).
[95] Song L, Guo T, Chen C. Experimental and numerical study of a self-centering prestressed concrete moment resisting frame connection with bolted web friction devices: self-centering prestressed concrete MRF connection with bolted WFDS. Earthq Eng Struct Dyn 2014;43:529–45. doi:10.1002/eqe.2358.
[96] Pekau OA, Guimond R. Controlling seismic response of eccentric structures by friction dampers. Earthq Eng Struct Dyn 1991;20:505–21. doi:10.1002/eqe.4290200602.
[97] Morgen BG, Kurama YC. A friction damper for post-tensioned precast concrete moment frames. PCI J 2004;49:112–33. doi:10.15554/pcij.07012004.112.133.
[98] Ferrara L, Felicetti R, Toniolo G, Zenti C. Friction dissipative devices for cladding panels in precast buildings: an experimental investigation. Eur J Environ Civ Eng 2011;15:1319–38. doi:10.1080/19648189.2011.9714857.
[99] Cherry S, Filiatrault A. Seismic response control of buildings using friction dampers. Earthq Spectra 1993;9:447–66. doi:10.1193/1.1585724.
[100] Dal Lago B, Biondini F, Toniolo G. Friction-based dissipative devices for precast concrete panels. Eng Struct 2017;147:356–71. doi:10.1016/j.engstruct.2017.05.050.
[101] Koshikawa T. Moment and energy dissipation capacities of post-tensioned precast concrete connections employing a friction device. Eng Struct 2017;138:170–80. doi:10.1016/j.engstruct.2017.02.012.
[102] Yildirim S, Asik G, Erkus B, Tonguc Y, Mualla I. Seismic retrofit of single story precast reinforced concrete structures with infill walls using friction dampers. In: Proceedings of the second European conference on earthquake engineering and seismoilogy; 2014. p. 10.
[103] Eldin MN, Dereje AJ, Kim J. Seismic retrofit of RC buildings using self-centering PC frames with friction-dampers. Eng Struct 2020;208:109925. doi:10.1016/j.engstruct.2019.109925.
[104] Naeem A, Kim J. Seismic retrofit of 3000 kVA power transformer using friction dampers and prestressed tendons. Structures 2021;32:641–50. doi:10.1016/j.istruc.2021.03.029.
[105] Cui Y, Tang Q, Wu T, Wang T. Seismic performance of bending-type frictional steel truss coupling beams. Earthq Eng Struct Dyn 2022;51:673–87. doi:10.1002/eqe.3585.
[106] Cui Y, Tang Q, Wu T, Okazaki T, Wang T. Mechanism and experimental validation of frictional steel truss coupling beams. J Struct Eng 2022;148:04022129. doi:10.1061/(ASCE)ST.1943-541X.0003420.
[107] Pall AS, Mash C. Seismic response of friction damped braced frames. J Struct Eng 1983;109:1334 –1334. doi:10.1061/(ASCE)0733-9445(1983)109:5(1334).
[108] Filiatrault A, Cherry S. Performance evaluation of friction damped braced steel frames under simulated earthquake loads. Earthq Spectra 1987;3:57–78. doi:10.1193/1.1585419.
[109] Aiken I.D., Kelly J.M., Pall A.S. Seismic response of a nine-story steel frame with friction damped cross-bracing. NZSEE, NZSEE; 1988.
[110] Anagnostides G. Design of economical means of enhancing the energy-absorption capability of braced frame structures. PhD. Imperial London College, 1988.
[111] Anagnostides G, Hargreaves AC. Shake table testing on an energy absorption device for steel braced frames. Soil Dyn Earthq Eng 1990;9:120–40. doi:10.1016/S0267-7261(09)90012-4.
[112] FitzGerald TF, Anagnos T, Goodson M, Zsutty T. Slotted bolted connections in aseismic design for concentrically braced connections. Earthq Spectra 1989;5:383–91. doi:10.1193/1.1585528.
[113] Giacchetti R, Whittaker AS, Bertero VV, Aktan HM. Seismic response of a DMRSF retrofitted with friction slip devices. International meeting on base isolation and passice enrgy dissipation. In: Proceedings of the international meeting on base isolation and passice enrgy dissipation; 1989.
[114] Tremblay R. Seismic behavior and design of friction concentrically braced frames for steel buildings. University of British Columbia; 1993. doi:1014288/10050464.
[115] Grigorian CE, Yang TS, Popov EP. Slotted bolted connection energy dissipators. Earthq Spectra 1993;9:491–504. doi:10.1193/1.1585726.
[116] Grigorian CE, Popov EP. Energy dissipation with slotted bolted connections. USA: Pacific Earthquake Engineering Research Center; 1994.
[117] Khoo H-H, Clifton C, Butterworth J, MacRae G, Ferguson G. Influence of steel shim hardness on the Sliding Hinge Joint performance. J Constr Steel Res 2012;72:119–29. doi:10.1016/j.jcsr.2011.11.009.
[118] Bagheri H, Hashemi A, Zarnani P, Quenneville P, Yan Z, Clifton GC, et al. A low–damage steel structure using resilient slip friction joint for a full-scale shaking table test. In: Proceedings of the 17th world conference on earthquake engineering (17WCEE); 2020. p. 12.
[119] Chanchi Golondrino JC, MacRae GA, Chase JG, Rodgers GW, Clifton GC. Seismic behaviour of symmetric friction connections for steel buildings. Eng Struct 2020;224:111200. doi:10.1016/j.engstruct.2020.111200.
[120] Chanchi Golondrino JC, MacRae GA, Chase JG, Rodgers GW, Scott ACN, Clifton GC. Steel building friction connection seismic performance – corrosion effects. Structures 2019;19:96–109. doi:10.1016/j.istruc.2018.11.008.
[121] Golondrino J.C., MacRae G.A., Chase J.G., Rodgers G.W., Clifton G.C. Applications of brake pads on asymmetrical friction connections (AFC). NZSEE, NZSEE; 2013, p. 8.
[122] MacRae GA, Zhao X, Jia L, Clifton GC, Dhakal R, Xiang P, et al. The China-NZ ROBUST friction building shaking table testing overview. In: Proceedings of the 17 th world conference on earthquake engineering; 2020. p. 10. 17WCEE.
[123] Ramhormozian S., Clifton G.C., MacRae G.A. The asymmetric friction connection with belleville springs in the sliding hinge joint. NZSEE, NZSEE; 2014, p. 10.
[124] Petty G. Evaluation of a friction component for a post-tensioned steel connection. PhD. Lehigh University, 1999.
[125] Tsai KC, Chou CC, Lin CL, Chen PC, Jhang SJ. Seismic self-centering steel beam-to-column moment connections using bolted friction devices. Earthq Eng Struct Dyn 2008;37:627–45. doi:10.1002/eqe.779.
[126] Kim HJ, Christopoulos C. Friction damped posttensioned self-centering steel moment-resisting frames. J Struct Eng 2008;134:1768–79. doi:10.1061/(ASCE)0733-9445(2008)134:11(1768).
[127] Wolski M, Ricles JM, Sause R. Experimental study of a self-centering beam–column connection with bottom flange friction device. J Struct Eng 2009;135:479–88. doi:10.1061/(ASCE)ST.1943-541X.0000006.
[128] Lin Y-C, Sause R, Ricles J. Seismic performance of a large-scale steel self-centering moment-resisting frame: MCE hybrid simulations and quasi-static pushover tests. J Struct Eng 2013;139:1227–36. doi:10.1061/(ASCE)ST.1943-541X.0000661.
[129] Filiatrault A. Analytical predictions of the seismic response of friction damped timber shear walls. Earthq Eng Struct Dyn 1990;19:259–73. doi:10.1002/eqe.4290190209.
[130] Li Z, Chen F, He M, Zhou R, Cui Y, Sun Y, et al. Lateral performance of self-centering steel–timber hybrid shear walls with slip-friction dampers: experimental investigation and numerical simulation. J Struct Eng 2021;147:04020291. doi:10.1061/(ASCE)ST.1943-541X.0002850.
[131] Loo WY, Kun C, Quenneville P, Chouw N. Experimental testing of a rocking timber shear wall with slip-friction connectors. Earthq Eng Struct Dyn 2014;43:1621–39. doi:10.1002/eqe.2413.
[132] Tyler RG. Test on a brake lining damper for structures. Bull N Z Soc Earthq Eng 1985.
[133] Aiken I.D., Kelly J.M. Earthquake simulator testing and analytical studies of two energy-absorbing systems for multistory structures. Pacific Earthquake Engineering Research Center; 1990.
[134] Aiken ID, Nims DK, Whittaker AS, Kelly JM. Testing of passive energy dissipation systems. Earthq Spectra 1993;9:335–70. doi:10.1193/1.1585720.
[135] Nims DK, Richter PJ, Bachman RE. The use of the energy dissipating restraint for seismic hazard mitigation. Earthq Spectra 1993;9:467–89. doi:10.1193/1.1585725.
[136] Filiatrault A, Tremblay R, Kar R. Performance evaluation of friction spring seismic damper. J Struct Eng 2000;126:491–9. doi:10.1061/(ASCE)0733-9445(2000)126:4(491).
[137] Chi B., Uang C.M. Dynamic testing of full-scale slotted bolted connections. Department of Structural Engineering: University of California San Diego; 2000.
[138] Jaisee S, Yue F, Ooi YH. A state-of-the-art review on passive friction dampers and their applications. Eng Struct 2021;235:112022. doi:10.1016/j.engstruct.2021.112022.
[139] Sun T, Peng L, Ji X, Li X. Development of a negative stiffness friction damping device with an amplification mechanism. Eng Struct 2023;275:115286. doi:10.1016/j.engstruct.2022.115286.

[140] Shirai K, Ito T, Kikuchi M. Seismic response control effects for reinforced-concrete buildings incorporating a passive variable friction device. J Build Eng 2022;62:105388. doi:10.1016/j.jobe.2022.105388.
[141] Zhu S. Seismic behavior of framed structural systems with self-centering friction damping braces. PhD. Lehigh University, 2007.
[142] Christopoulos C, Tremblay R, Kim HJ, Lacerte M. Self-centering energy dissipative bracing system for the seismic resistance of structures: development and validation. J Struct Eng 2008;134:96–107. doi:10.1061/(ASCE)0733-9445(2008)134:1(96).
[143] Erochko J, Christopoulos C, Tremblay R. Design and testing of an enhanced-elongation telescoping self-centering energy-dissipative brace. J Struct Eng 2015;141:04014163. doi:10.1061/(ASCE)ST.1943-541X.0001109.
[144] Chou CC, Chen YC. Development of steel dual-core self-centering braces: quasi-static cyclic tests and finite element analyses. Earthq Spectra 2015;31:247–72. doi:10.1193/082712EQS272M.
[145] Asfaw AM, Cao L, Ozbulut OE, Ricles J. Development of a shape memory alloy-based friction damper and its experimental characterization considering rate and temperature effects. Eng Struct 2022;273:115101. doi:10.1016/j.engstruct.2022.115101.
[146] Yang TY, Moehle JP, Bozorgnia Y, Zareian F, Wallace JW. Performance assessment of tall concrete core-wall building designed using two alternative approaches. Earthq Eng Struct Dyn 2012;41:1515–31. doi:10.1002/eqe.2219.
[147] Sarkisian M., Long E., Hassan W. Performance-based engineering of core wall tall buildings. Proceedings of the ASCE Structures Congress 2013, Pittsburgh, Pennsylvania, United States : American Society of Civil Engineers; 2013, p. 1094–108. 10.1061/9780784412848.097.
[148] Li G-Q, Pang M, Sun F, Jiang J, Hu D. Seismic behavior of coupled shear wall structures with various concrete and steel coupling beams. Struct Des Tall Spec Build 2018;27:e1405. doi:10.1002/tal.1405.
[149] Tauberg N., Kolozvari K., Wallace J. Ductile reinforced concrete coupled walls: FEMA P695 study. 2018.
[150] Mavros M, Panagiotou M, Koutromanos I, Alvarez R, Restrepo JI. Seismic analysis of a modern 14-story reinforced concrete core wall building system using the BTM-shell methodology. Earthq Eng Struct Dyn 2021. doi:10.1002/eqe.3627.
[151] FEMA. NEHRP recommended seismic provisions: design examples, training materials, and design flow charts. 2021.
[152] Brown JR, Li M, Palermo A, Pampanin S, Sarti F. Experimental testing of a low-damage post-tensioned C-shaped CLT Core-Wall. J Struct Eng 2021;147:04020357. doi:10.1061/(ASCE)ST.1943-541X.0002926.
[153] Bruneau M, Kizilarslan E, Varma AH, Broberg M, Shafaei S, Seo J. R-Factors for coupled composite plate shear walls /Concrete filled (CC-PSW/CF). Charles Pankow Foundation; 2019.
[154] Agrawal S, Broberg M, Varma A. Seismic design coefficients for speedcore or composite plate shear walls - concrete filled. Purdue University; 2020.
[155] American Institute of Steel Construction. SpeedCore |American Institute of Steel Construction 2022. https://www.aisc.org/why-steel/innovative-systems/SpeedCore/(accessed December 13, 2022).
[156] Moehle J.P., Ghodsi T., Hooper J.D., Fields D.C., Gedhada R. Seismic design of cast-in-place concrete special structural walls and coupling beams, 2012
[157] Calugaru V, Panagiotou M. Response of tall cantilever wall buildings to strong pulse type seismic excitation. Earthq Eng Struct Dyn 2012;41:1301–18. doi:10.1002/eqe.1185.
[158] Van Den Einde L, Conte JP, Restrepo JI, Bustamante R, Halvorson M, Hutchinson TC, et al. NHERI@UC San Diego 6-DOF large high-performance outdoor shake table facility. Front Built Environ 2021;6:181. doi:10.3389/fbuil.2020.580333.
[159] ScanPac Friction & phenolic specialists. ScanPac https://www.scanpac.com/(accessed December 5, 2022).
[160] ANSYS. Academic research mechanical 2022.
[161] McKenna F, Fenves G, Michael S. The opensees command language manual. Pacific Earthquake Engineering Center, University of California Berkeley; 2000.
[162] ASCE Minimum design loads. 7th ed. Reston, VA: ASCE; 2017. doi:10.1061/9780784414248.